Magmatic history and evolution of the Central American Land Bridge in Panama since Cretaceous times

Wencke Wegner[1,†], Gerhard Wörner[1], Russell S. Harmon[2], and Brian R. Jicha[3]
[1]*Division of Geochemistry, Geosciences Center, University of Göttingen, 37077 Göttingen, Germany*
[2]*U.S. Army Research Laboratory Army Research Office, Durham, North Carolina 27703, USA, and Department of Marine, Earth, and Atmospheric Sciences, North Carolina State University, Raleigh, North Carolina 27695, USA*
[3]*Department of Geology and Geophysics, University of Wisconsin, Madison, Wisconsin 53706, USA*

ABSTRACT

Chemical compositions for 310 igneous rocks from the Cordillera de Panama and the Soná and Azuero peninsulas were supplemented by $^{40}Ar/^{39}Ar$ dating and Sr-, Nd-, Pb-, and O-isotope analysis to determine the magmatic evolution and oceanic plate interactions over the past 100 Ma in western Panama. An initial phase of intraplate magmatism, having geochemical characteristics of the Galápagos hotspot, formed the oceanic basement of the Caribbean large igneous province from 139 to 69 Ma. Younger accreted terranes with enriched trace element patterns (accreted ocean island basalt [OIB]) were amalgamated between 70 and 20 Ma. A second magmatic phase in the Azuero and Soná peninsulas has trace element patterns (Soná-Azuero arc) suggesting the initiation of subduction at 71–69 Ma. Arc magmatism continued in the Chagres basin region (Chagres-Bayano arc) from 68 to 40 Ma. A third phase formed discrete volcanic centers across the Cordillera de Panama (Cordilleran arc) from 19 to 5 Ma. The youngest phase consists of isolated volcanic centers of adakitic composition (Adakite suite) in the Cordillera de Panama that developed over the past 2 million years.

Initiation of arc magmatism at 71 Ma coincides with the cessation of Galápagos plateau formation, suggesting a causal link. The transition from intraplate to arc magmatism occurred relatively quickly and introduced a new enriched mantle source. The arc magmatism involved progressive transition to more homogeneous intermediate mantle wedge compositions through mixing and homogenization of subarc magma sources through time and/or the replacement of the mantle wedge by a homogeneous, relatively undeleted asthenospheric mantle. Adakite volcanism started after a magmatic gap, enabled by the formation of a slab window.

INTRODUCTION AND GEOLOGICAL SETTING

The Central American Land Bridge (Fig. 1) is located between Nicaragua and northern Colombia and occupies a critical position connecting the continents of North America and South America. Its formation around 3 million years ago (Coates et al., 2000, 1992) was a consequence of Caribbean regional tectonics possibly combined with interaction of the paleo-Galápagos hotspot tracks with the Central American subduction zone (Hoernle et al., 2002) and had significant effects on marine and terrestrial faunal distributions and global oceanic circulation patterns (Duque-Caro, 1990; Coates et al., 1992; Collins et al., 1996; Haug and Tiedemann, 1998).

The plate tectonic history of the region has been reviewed by Pindell et al. (2006), who postulate a Pacific origin of the Caribbean plate and significant displacement since Cretaceous time relative to the westward-moving North American and South American plates. Arc magmatism, together with high-P/low-T metamorphic rocks, dates the onset of westward-dipping subduction at the eastern margin of the Caribbean plate that resulted from a relative eastward movement of the Pacific region at 125–113 Ma (Pindell et al., 2005, 2006). An Aleutian-style transcurrent plate boundary at the eastern margin of the Pacific (Farallon) plate was converted into a west-facing subduction zone that subsequently changed to be east-facing during Aptian time. The initial Greater Antilles arc and the present Lesser Antilles subduction zone were a consequence of this convergence at the eastern margin of the Caribbean plate. The western plate margin may have been inactive until the time when eastward-facing subduction commenced between the Pacific and Caribbean plates, probably by Late Albian time (~95 Ma; Pindell et al., 2006). The origin and the role of the thickened Caribbean plateau have been much debated. Some authors (e.g., Duncan and Hargraves, 1984) have suggested that the plateau formed as a result of the arrival of the Galápagos plume below the Pacific plate and subsequent development of the Caribbean large igneous province on Jurassic oceanic crust. This over-thickened crust caused choking of Pacific subduction and initiated the west-facing subduction (e.g., Kerr et al., 2002; Hauff et al., 1997, 2000a). Pindell et al. (2005, 2006), however, argued that an age of 92–88 Ma for rocks of the Caribbean plateau is inconsistent with older high-pressure and/or low-temperature rocks that suggest an earlier subduction reversal. However, Hoernle et al. (2004) published six Ar-Ar ages for Caribbean large igneous province rocks from the Nicoya Peninsula in the range of 139 to 110 Ma that would permit an older age for the plateau, thus reviving the idea of a possible link between Galápagos and Caribbean large igneous province. This result opens the possibility that plateau formation began at this early time, caused the subduction reversal at ~110 Ma (Pindell et al., 2005), and then continued to develop until ~69 Ma (Hoernle et al., 2004) well after the initiation of convergence on its eastern margin.

The geochemical composition and the age (139–69 Ma, Hoernle et al., 2004) of the Caribbean large igneous province mafic complexes, along the Central American Land Bridge between the Santa Elena transform fault (i.e., the southern tectonic border to the Chortis continental block that contained present-day Guatemala, Honduras, and most of Nicaragua) in the north, and the Atrato fault (the continuation of the south Caribbean fault along the northern margin of South America) in the south, have been

[†]E-mail: wwegner1@gwdg.de

GSA Bulletin; March/April 2011; v. 123; no. 3/4; p. 703–724; doi: 10.1130/B30109.1; 13 figures; 5 tables; Data Repository item 2010101.

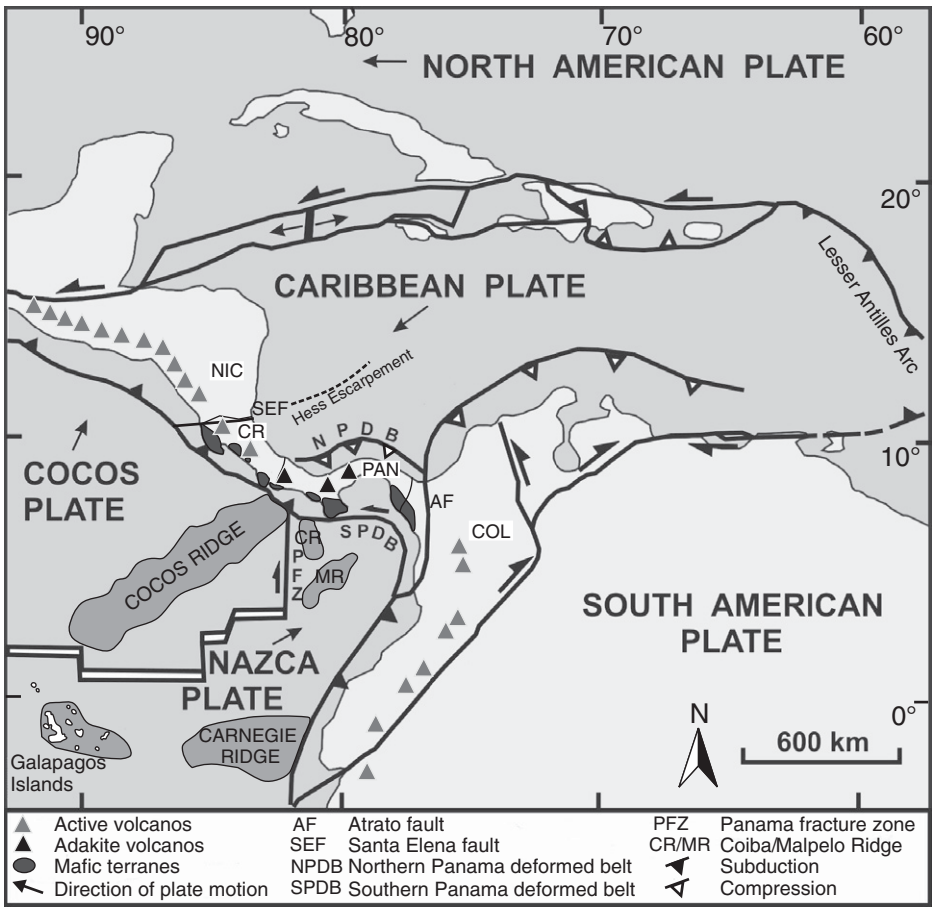

Figure 1. Tectonic setting of the Central American Land Bridge region (after Meschede and Frisch, 1998). COL—Colombia, CR—Costa Rica, NIC—Nicaragua, PAN—Panama.

taken as evidence of the important role of the Galápagos hotspot for the development of the Central American Land Bridge (Hauff et al., 2000a, 2000b; Hoernle et al., 2002). These mafic terranes either comprise a major part of the Central American crust or are fragments amalgamated tectonically to the Chortis block (Goossens et al., 1977; Reynaud et al., 1999). However, the link between the Galápagos hotspot and these terranes remains disputed. Pindell et al. (2006) argue, based on absolute plate motion reconstruction, that linking Galápagos to these terranes would require migration of the Galápagos hotspot some 1000 km within the fixed mantle reference frame. Therefore, the tectonic history of the western margin of Caribbean plate requires continued investigation.

Magmatic rocks in Panama and Costa Rica have been formed by subduction zone volcanism since early Tertiary time (64 or 61 Ma, Maury et al. [1995] and Lissinna et al. [2006], respectively). A broad temporal change in magma compositions from tholeiitic to (low-K) calc-alkaline has been observed beginning in the Oligocene (since >30 Ma) by Alvarado et al. (1992), de Boer et al. (1995), and Abratis and Wörner (2001). This change continued from low-K calc-alkaline toward high-K calc-alkaline compositions, which started between the middle and late Miocene (Gazel et al., 2009). During this time, additional ocean island basalt (OIB)–type basalt complexes, derived from seamounts related to the Galápagos hotspot, were accreted to the continental margin until ~16 Ma (Alvarado et al., 1992; Hauff et al., 1997, 2000a; Hoernle et al., 2002). Typical arc volcanism in southern Costa Rica and western Panama ceased during the upper Miocene due to the collision of the Cocos Ridge with the Chortis block. This collision took place at 2–3 Ma (MacMillan et al., 2004). This was followed by a 2–3 million year gap in magmatic activity. At the same time, spreading ceased in the Panama basin (Lonsdale and Klitgord, 1978) and subduction also stopped on the Pacific coast of eastern and central Panama, but continued plate convergence was accommodated by movements in the N-S–striking Panama fracture zone and the eastern and northern Panama deformed belt (Mann and Kolarsky, 1995). The progressive closure of the oceanic connection between the Caribbean Sea and Pacific Ocean occurred during the interval between 6.2 and 3.5 Ma (Duque-Caro, 1990; Coates et al., 1992; Collins et al., 1996; Haug et al., 2001; Coates et al., 2000) as a consequence of terrane collision, magmatism, and tectonic uplift (Hoernle et al., 2002; de Boer et al., 1995) along transverse fault systems in present-day central Panama. Subsequently, volcanism of adakitic composition was initiated in western Panama and southern Costa Rica at ~2 Ma (Defant et al., 1991a, 1991b; Johnston and Thorkelson, 1997; Abratis and Wörner, 2001); its source and petrogenesis remain controversial.

Previous geochemical studies on volcanic rocks of the Central American Land Bridge region have focused on three main issues: (1) the origin of the mafic (Caribbean large igneous province and "younger") complexes (Goossens et al., 1977; Hauff et al., 1997, 2000a; Hoernle et al., 2002, 2004 and references therein; Hoernle and Hauff, 2007), (2) the subsequent evolution of Paleocene–Miocene age rocks on the western Caribbean margin having a volcanic arc affinity, and (3) the tectonic context and origin of Quaternary volcanic centers in western Panama and Costa Rica (de Boer et al., 1988, 1995; Defant et al., 1991a, 1991b; Drummond et al., 1995; Abratis and Wörner, 2001; Carr et al., 2003). However, the link between the Caribbean large igneous province basement and the volcanic arc setting, i.e., Paleocene to Miocene volcanism, has received relatively little attention (de Boer et al., 1988, 1995) due to limited exposure and difficult access to the Central American Cordillera.

Based on existing data related to the magmatic history of southern Central America, this study fills an important knowledge gap by providing new high-resolution $^{40}Ar/^{39}Ar$ dates, major and trace element analyses, and Nd-, Sr-, Pb-, and O-isotope ratios for a large suite of volcanic and intrusive rocks from western and central Panama that document the magmatic history and petrogenetic evolution of the Central American Land Bridge region over the past 71 million years. This study examines the temporal evolution of magma compositions and variations in associated magma sources during this period and discusses the tectonic processes which led to these changes.

SAMPLE COLLECTION AND ANALYTICAL METHODS

Figure 2 shows the geographic locations of the samples analyzed. The study area extends over an E-W distance of ~500 km across the

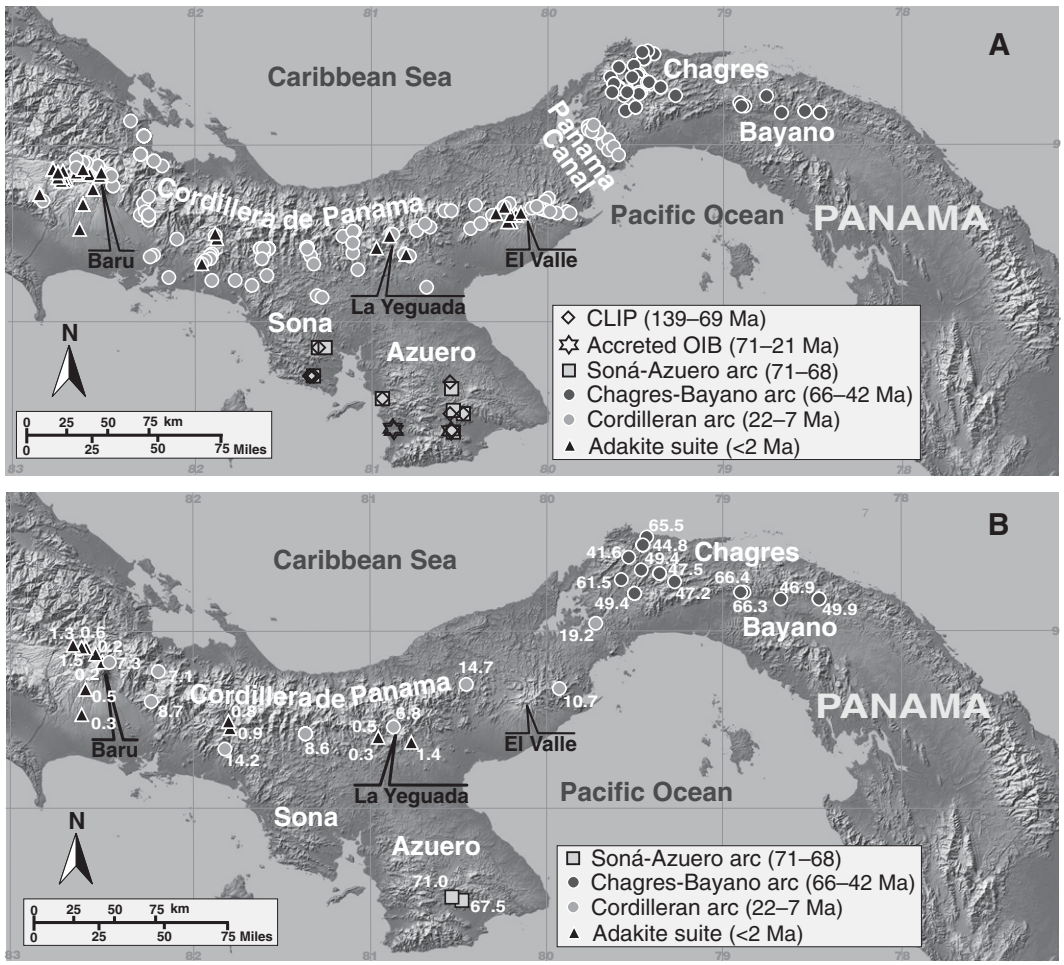

Figure 2. Topographic map of Panama showing the locations and volcanic features referred to in the text and the geographic distribution of the samples (A: all samples studied, B: only dated samples with labeled ages) collected for this study. The symbols (explained in the figure) represent the different arc groups sampled.

Central Cordillera of Panama from the Lake Bayano region in the east to the Costa Rican border in the west (Fig. 2). Samples were also collected in a NW-SE traverse along the Panama Canal, throughout the Upper Rio Chagres region northeast of the Panama Canal, and from the Azuero and Soná peninsulas in southern Panama. The majority of the samples are volcanic and plutonic rocks of Upper Cretaceous to Quaternary age, but also include some samples from the Cretaceous basement. The samples are divided into six geographic-temporal groups (Caribbean large igneous province, accreted OIB, Soná-Azuero arc, Chagres-Bayano arc, Cordilleran arc, and Adakite suite) on the basis of age, spatial distribution, and trace element characteristics (see discussion that follows).

Only the freshest rocks were sampled in the field. However, many samples exhibited minor but noticeable degrees of alteration. 310 samples were selected for geochemical analysis at the Geosciences Center at the University of Göttingen by X-ray fluorescence spectroscopy (XRF) and inductively coupled plasma–mass spectrometry (ICP-MS). Based on mineral content, lithology, and presumed age from geological field relations, subsets of 40 samples (rocks and separated dated minerals) were selected for determination of isotopic composition ($^{87}Sr/^{86}Sr$, $^{143}Nd/^{144}Nd$, $^{206}Pb/^{204}Pb$, $^{207}Pb/^{204}Pb$, $^{208}Pb/^{204}Pb$, and $^{18}O/^{16}O$ ratios) representing all lithologies and age groups. Separated clean, acid-etched minerals (amphiboles, K-feldspars, and pyroxenes) were used for isotope analysis rather than whole rocks because clean minerals record magmatic values and should be less affected by alteration processes. Of these same minerals 35 were also used for age dating by the high-precision $^{40}Ar/^{39}Ar$ method at the University of Wisconsin–Madison Rare Gas Geochronology Laboratory. As a consequence of strong secondary alteration of rocks from the Soná-Azuero arc, only two samples from this group were suitable for isotopic analysis, whereas 14, 10, and 14 samples from the Chagres-Bayano arc, Cordilleran arc, and Adakite suite groups, respectively, were analyzed for isotopic composition.

Concentrations of major and minor elements (Si, Ti, Al, Fe, Mn, Mg, Ca, Na, K, and P) as well as selected trace elements (Nb, Zr, Y, Sr, Rb, Ga, Zn, Cu, Ni, Co, Cr, V, Ba, and Sc) were analyzed by XRF on glass fusion disks on a PANalytical AXIOS X-ray fluorescence spectrometer. About 50 reference materials from the U.S. Geological Survey; the International Working Group on Analytical Standards of Minerals, Ores and Rocks; the National Research Council of Canada; the Geological Survey of Japan; the South African Bureau of Standards; and the U.S. National Institute of Standards and Technology (NIST) were used for the major and trace element calibration. For major element analyses, analytical precision is better than 1%–2%; for trace element determinations standard deviations of consecutive analyses are in the range of 2% to 5% relative at the level of 20–30 ppm. Detection limits vary from 3 to 0.5 ppm for the majority of the measured elements.

Rare-earth elements (REE; La and Lu), high-field-strength elements (HFSE; Nb, Ta, Zr, and Hf), large-ion-lithophile elements (Rb, Sr, Ba, and Cs), and a group of other trace elements (Li, Sc, Cu, V, Cr, Co, Ni, Zn, Y, Pb, Th, and U) were measured using a Perkin Elmer

ELAN DRCII ICP-MS. Sample solutions were prepared following an approach modified from Heinrichs and Herrmann (1990) and diluted to 1:1000 with 20 ppb Ge, Rh, Re, and In as internal standards. Based on co-processing the laboratory internal standards and the international standards JB-3 and JA-2 as unknown samples, the 2σ error of the analytical method was estimated to be <20% for Nb and Ta, <10% for Be, Cs, Cu, Hf, Li, Y, Rb, Pb, Tl, Th, and U, and ~5% for the REE.

Isotope ratios of $^{87}Sr/^{86}Sr$, $^{143}Nd/^{144}Nd$, $^{206}Pb/^{204}Pb$, $^{207}Pb/^{204}Pb$, and $^{208}Pb/^{204}Pb$ were measured using a Finnigan MAT262-RPQII thermal ionization mass spectrometer (TIMS). For Sr-, Nd-, and Pb-isotope ratio determinations, 30 mg of hand-picked feldspar and 50 mg of amphibole were leached with 1 ml of 0.18N HCl at 50 °C and 100 °C, each for 15 min and dissolved in 4 ml of HF:HNO_3 (1:1) for 24 h at 200 °C in Savillex beakers inside a pressure vessel. For Sr separation we used columns containing BIORAD AG 50W-X8, 200–400 mesh ion exchange resin. For Nd separation, the REE fraction of the first separation step was separated in a second set of columns filled with Teflon powder impregnated with ion-exchanging HDEHP bis-(2-etylhexy)-phosphate. For TIMS measurements, the separated Sr and Nd was dissolved in 3 µl HNO_3 and 3 µl H_3PO_4 and loaded on Re double filaments (~1 µg). Measured Sr- and Nd-isotope ratios were corrected for mass fractionation to $^{87}Sr/^{86}Sr = 0.1194$ and $^{143}Nd/^{144}Nd = 0.7219$ and normalized to values for the NIST standard reference materials (SRMs) ($^{87}Sr/^{86}Sr = 0.710245$), and La Jolla ($^{143}Nd/^{144}Nd = 0.511847$) standards. Measured values of these standards over the period of the study were $^{87}Sr/^{86}Sr = 0.710258 \pm 7$ (10 analyses) and $^{143}Nd/^{144}Nd = 0.511848 \pm 5$ (10 analyses). External 2σ errors are estimated at <0.004% for Sr and Nd. The total blank for Sr was 261 pg and for Nd 135 pg and thus considered negligible. For Pb-isotope analysis, separation ~100 mg of leached minerals were dissolved in 4 ml HF:HNO_3 (1:1) in Savillex pressure vessels at 200 °C for at least 12 h. After pressure digestion and evaporation, the samples were dissolved twice in 1 ml 0.5N HBr and centrifuged. Pb was separated on anion exchange columns containing resin (Biorad AG1-X8, 200–400 mesh). The Pb fraction was mounted on Re single filament using 3 µl HNO_3 and 3 µl silica-gel. Ionization temperature for Pb measurement was held constant between 1150 and 1300 °C and controlled by an optical temperature reader. Measured Pb-isotope ratios were corrected to NIST SRM-981 using a mass fractionation factor of 0.069% for $^{206}Pb/^{204}Pb$, 0.077% for $^{207}Pb/^{204}Pb$, and 0.049% for $^{208}Pb/^{204}Pb$. Thirteen standard measurements gave means of $^{206}Pb/^{204}Pb = 16.92 \pm 0.04$, $^{207}Pb/^{204}Pb = 15.47 \pm 0.04$, and $^{208}Pb/^{204}Pb = 37.63 \pm 0.09$. The total error (2σ) was <0.1%. The total blank for Pb was 500 pg.

$^{18}O/^{16}O$ ratios were determined on one to three grains (~1 mg) of amphibole, pyroxene, or feldspar using a Thermo MAT 253 dual-inlet, gas-source mass spectrometer. The gas extraction line used is similar to that described by Sharp (1990) except that F_2 is used for fluorination instead of BrF_5 and that O_2 is measured directly and not reacted to CO_2. Twelve samples and four standards were loaded into a Ni sample holder and evacuated overnight. The samples were heated (>2000 °C) by a CO_2 laser in an atmosphere of F_2, liberating molecular oxygen and forming residual fluorides. Excess F_2 was then removed by reaction with NaCl at ~150 °C to form NaF, and any Cl_2 produced was collected in two liquid nitrogen traps at –196 °C. Finally, purified O_2 was trapped on a molecular sieve at –196 °C and the O_2 then expanded into the mass spectrometer inlet system for the simultaneous analysis of masses 32, 33, and 34 by heating the molecular sieve to ~80 °C. The sample gas is compared to a reference O_2 of known $\delta^{18}O_{VSMOW}$ (Vienna standard mean ocean water) of +12.5‰ to determine its O-isotopic composition. For further details, see Pack et al. (2007). Measured $\delta^{18}O$ values were corrected for machine drift by normalization to measured standards (National Bureau of Standards [NBS] 28 quartz, San Carlos olivine, UWG-2 garnet).

Incremental heating experiments for $^{40}Ar/^{39}Ar$ analysis were performed on amphibole, K-feldspar, plagioclase crystals, and matrix material in the Rare Gas Geochronology Laboratory at the University of Wisconsin–Madison using a defocused 25 W CO_2 laser. Individual grains were analyzed from four samples, but in most cases, multicrystal aliquots (~10 mg) were lased to yield sufficient argon for analysis. Prior to each laser step-heating experiment, samples were pre-degassed at 2.0% power (0.06 W) to remove potentially large amounts of water and atmospheric argon. Very little ^{39}Ar (<0.1% of total ^{39}Ar in the sample) is released during this pre-heating procedure. Experiments yielded largely concordant age spectra with four to ten steps comprising >82% of the gas released. Isotopic analyses and data reduction followed the procedures of Smith et al. (2006). Details of the method and results are given in the supplementary material complete Ar results (see GSA Data Repository[1]).

[1]GSA Data Repository item 2010101, a detailed map of the sample regions and the complete Ar/Ar results as well as a full data table for major- and trace elements, is available at http://www.geosociety.org/pubs/ft2010.htm or by request to editing@geosociety.org.

RESULTS AND DISCUSSION

The results of the 310 chemical analyses and their locations are given in the supplementary material full data table and location map (see footnote 1). Our Caribbean large igneous province and accreted OIB groups were defined based on regional geology and similarities to published trace element data (Hauff et al., 2000a; Hoernle et al., 2002). The other groups are defined on the basis of stratigraphy and field morphology of sampled units, together with petrology and spatial vicinity of the dated samples of the same group. To ensure that our sample grouping indeed represents mostly time rather than only regional geographic distribution, dated and undated samples of different groups were compared for chemical and isotopic similarities. The within-group consistency is much higher than the intergroup consistency of neighboring samples.

Most volcanic and plutonic rocks of western-central Panama are subalkaline in character (Figs. 3 and 4). Although care was taken to analyze only fresh samples, thin section examination has revealed minor degrees of secondary alteration in some samples. Therefore, some alkali values in the data table (full data table; see footnote 1) and Figures 3 and 4 may not be absolutely reliable due to the fact that these elements are easily affected by secondary alteration.

Major Element Geochemistry

The Caribbean large igneous province suite in Panama consists mainly of submarine flood basalts (43–51 wt% SiO_2) that are characteristic of the oceanic basement of the Caribbean plate generated between 139 and 69 Ma. Most Caribbean large igneous province basement samples are classified in Figure 4 as tholeiites following Rickwood (1989). The remaining five types are subdivided into two more subgroups on the basis of trace element patterns (Fig. 5). Accreted OIB denotes accreted ridges and ocean islands that have an enriched, intraplate geochemical signature (Alvarado et al., 1992; Hoernle et al., 2002). Also, there are some rare samples with an arc signature that have been found within the Caribbean large igneous province terranes in central and western Panama (Soná-Azuero arc), which are similar in composition to the Chagres-Bayano arc rocks.

The Chagres-Bayano arc is represented mostly by samples from the Upper Rio Chagres region located northeast of the Panama Canal (Wörner et al., 2005, 2009; Fig. 2). The Chagres Igneous Complex is an exposed section through a highly tectonized Late Cretaceous to mid-Tertiary submarine lava flow-dike complex, associated subvolcanic intrusive rocks (gabbros to

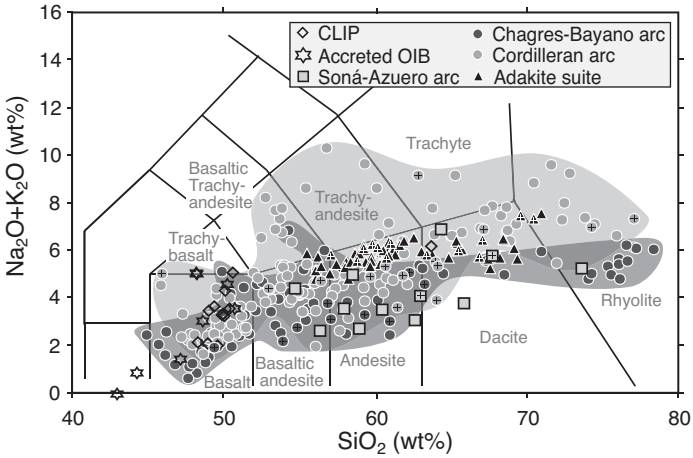

Figure 3. Chemical classification and nomenclature of volcanic rocks displayed in total alkali versus silica (TAS) diagram according to Le Maitre et al. (1989). Shaded areas highlight the two largest arc groups: dark gray for Chagres-Bayano arc and light gray for Cordilleran arc. Samples for which $^{40}Ar/^{39}Ar$ ages were obtained are denoted with crosses. CLIP—Caribbean large igneous province; OIB—ocean island basalt.

granites), and overlying and intercalated volcanic breccias. This magmatic sequence formed between 66 and 42 Ma (see discussion of age data below) and was previously grouped into the Caribbean large igneous province domain by previous workers (e.g., Hoernle et al., 2002 and others). However, as will be shown below based on trace element systematics, all rocks of the Chagres-Bayano region have a clear arc geochemical affinity.

We define a Cordilleran arc mostly based on the regional occurrence of deeply eroded volcanic edifices and their intrusive counterparts along the western Panamanian Cordillera that were originally described by de Boer et al. (1988) and Defant et al. (1991a, 1991b). Ages for rocks from the Cordilleran arc fall into the Oligocene to Miocene, which correspond to magmatic activity in southern Costa Rica around that time (Drummond et al., 1995). This group is mostly composed of lavas, dikes, and intrusives that are variably altered. However, fine-grained aphyric andesites also occur, which are particularly fresh and have been preferentially sampled.

The last sample group (Adakite suite) comprises a suite of andesitic to dacitic rocks (Fig. 3) from geographically scattered locations in central-western Panama that are associated with isolated stratovolcanoes in the Veraguas and Chiriquí provinces and occur as remnants of dacitic ignimbrites that span the Panama–Costa Rica border (Defant and Drummond, 1990; Defant et al., 1991a, 1991b; Johnston and Thorkelson, 1997; Abratis and Wörner, 2001). These rocks have 58–71 wt% SiO_2, steep heavy REE patterns, high $(Sm/Yb)_n$ ratios of 2.47–10.3, and are generally younger than 5 Ma (Fig. 5).

As illustrated in Figure 3, the three arc suites (Soná-Azuero arc, Chagres-Bayano arc, and Cordilleran arc) span the entire compositional range from basalt to rhyolite and from gabbro to granite (45 wt% to 78.5 wt% SiO_2). Samples from the Caribbean large igneous province and accreted OIB groups are mostly of basaltic composition, and most samples from the two older arc groups, Soná-Azuero arc and Chagres-Bayano arc, fall into the low-K array (Fig. 4A). A few analyses plot in the medium-K and high-K field, most likely as a consequence of secondary alteration, and thus these samples are not considered further. Considering only the dated, pristine samples, the Soná-Azuero arc and Chagres-Bayano arc plot only in the low-K and lower part of the medium-K array. The Cordilleran arc samples are extremely variable in K_2O content, spanning the range from low-K to shoshonitic compositions. Some of this scatter is likely due to alteration. Considering only the dated and pristine samples, the rocks of the Cordilleran arc plot exclusively in the medium K array (Fig. 4). Samples of the Adakite suite also show some scatter with respect to K_2O (Fig. 4A), but all adakite samples are fresh and unaltered, and the majority fall in the medium-K and high-K field (Fig. 4). It is not possible from our age data to precisely determine the timing

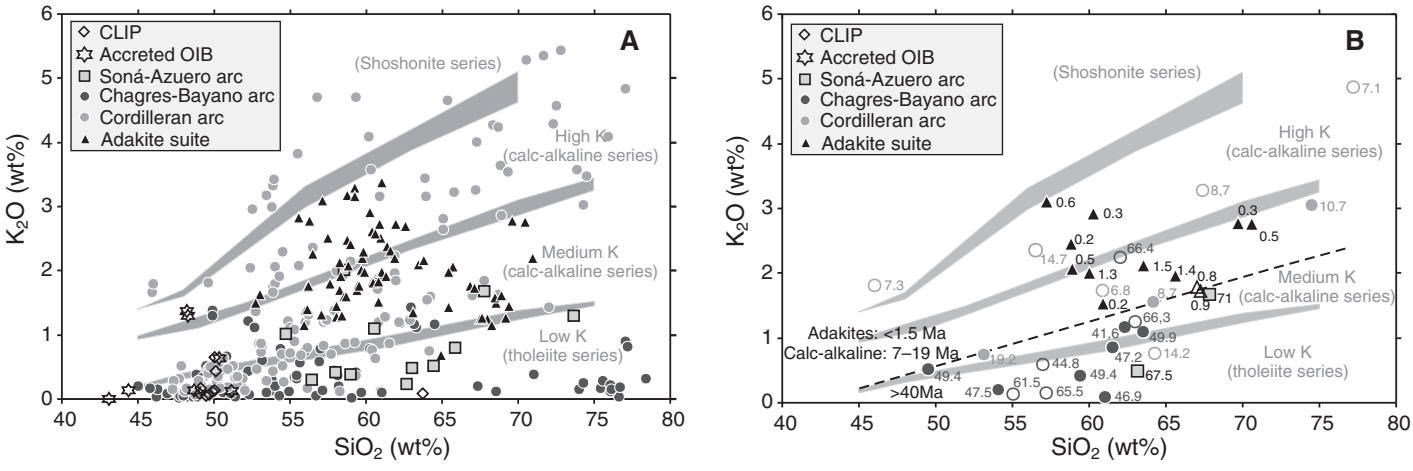

Figure 4. Subdivision of subalkaline rocks after Rickwood (1989) based on the basis of K_2O versus silica content: (A) all samples and (B) only dated samples. Open data symbols denote altered samples (see text for discussion). The numbers by the data points in (B) are the $^{40}Ar/^{39}Ar$ ages. CLIP—Caribbean large igneous province; OIB—ocean island basalt.

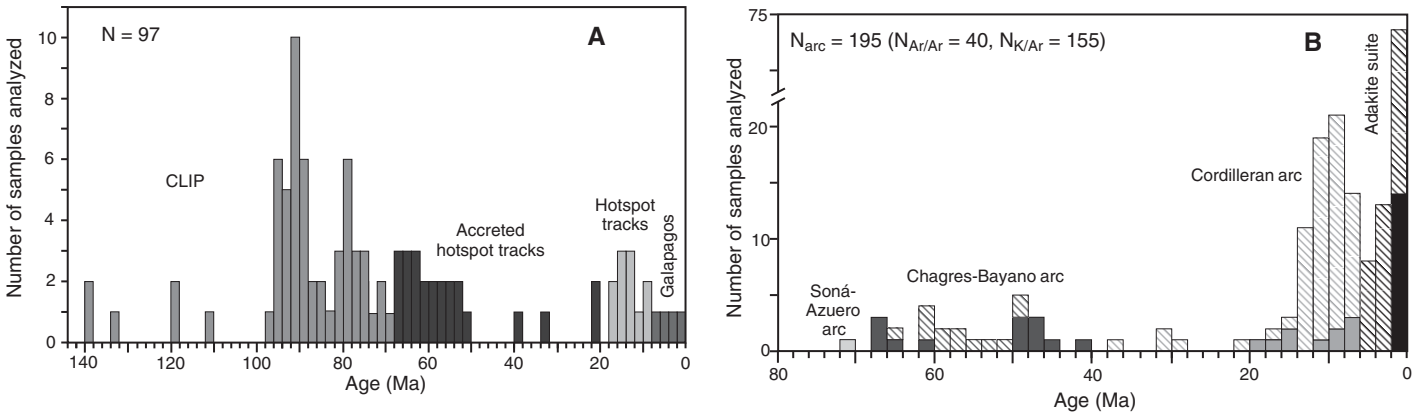

Figure 5. (A) Age distribution of Caribbean large igneous province rocks and Galápagos-derived seamounts (after Hoernle et al., 2004). Data sources: Alvarado et al. (1997); Christie et al. (1992); Hauff et al. (2000a); Hoernle et al. (2002, 2004); Kerr et al. (1997, 2002); Lapierre et al. (1999); Revillon et al. (2000a); Sinton et al. (1996, 1997, 1998); White et al. (1993). (B) Age distribution of arc rocks in central and western Panama and in southern Costa Rica; Gray bars—$^{40}Ar/^{39}Ar$ data from Abratis and Wörner (2001); black bars—this study; hatched bars—K/Ar data from Kesler et al. (1977); de Boer et al. (1991); Defant et al. (1991a, 1991b, 1992); Drummond et al. (1995); and Maury et al. (1995). CLIP—Caribbean large igneous province.

for the change from tholeiitic to calc-alkaline magmatism (Figs. 3 and 4). Rocks of the Soná-Azuero arc and Chagres-Bayano arc are mainly tholeiitic, but both groups contain some calc-alkaline samples. The Cordilleran arc is composed of both tholeiitic and calc-alkaline samples. No compositional evolution through time is seen within single rock suites. Therefore, it is likely that the change from largely tholeiitic to predominantly calc-alkaline magmatism took place at different times in different locations across Panama during Cordilleran arc magmatism. This is consistent with the general age pattern for volcanism in southern Costa Rica (MacMillan et al., 2004; and discussion below).

$^{40}Ar/^{39}Ar$ Dating

High-precision $^{40}Ar/^{39}Ar$ ages were determined for a subset of 35 samples. Plateau ages, determined by incremental heating are listed in Table 1 and displayed in histogram form in Figure 5 (see also complete Ar results [see footnote 1]). These samples span the entire range with respect to composition and geographic location across west-central Panama. Although K_2O values are relatively low in the whole rocks, precise dating of mineral separates of amphibole and K-feldspar was possible.

There now is sufficient geochronologic data to examine the temporal nature of magmatism across southern Central America over the past 100 million years. The small overlap in age between Caribbean large igneous province (>69 Ma) and arc rocks (<71 Ma) is shown in Figure 5; in fact, only two samples fall into the overlap interval between 69 and 71 Ma. Our oldest ages of 71–67.5 Ma for Soná-Azuero arc samples come from the Azuero and Soná peninsulas (Fig. 2). Thus, the age data strongly imply that subduction-related magmatism in Panama commenced ~71 million years ago in the vicinity of the Caribbean large igneous province complexes on the Azuero and Soná peninsulas, subsequently shifting into the Chagres region (Fig. 2) of the central Cordillera de Panama at 66 Ma (Fig. 5B). This conclusion is consistent with published K-Ar data (Kesler et al., 1977), stratigraphic evidence of Fisher and Pessagno (1965) and Weyl (1980), and a recent study by Buchs et al. (2007) who concluded that arc magmatism in Costa Rica and Panama was initiated in Late Cretaceous to early Tertiary time. However, Pindell et al. (2006) cite evidence from clasts in boreholes and detrital minerals in older sediments to suggest a possible onset of arc magmatism during Albian time ~95 Ma. However, because the latter evidence is scarce and not based on measured trace element character of these rocks, and because of the consistent and abundant age data discussed above, we conclude that a later onset of subduction in the western margin of the Caribbean plate at around 71 Ma is much more likely.

The oldest Chagres-Bayano arc rocks of the Cordillera de Panama (66 Ma) are found in the Chagres and Lake Bayano areas east of the Panama Canal (Fig. 2), but younger rocks of this group in the same region range in age down to 41.6 Ma (Table 1). Given the abundance of ages determined and the complete coverage of lithologies and their spatial distribution, the paucity of ages between 61.5 and 50 Ma in Figure 4 is interpreted to be geologically meaningful. Earlier (66.4–61.5 Ma) and later (49.4–41.6 Ma) magmatic suites within the Chagres-Bayano arc suite, however, are indistinguishable geochemically. Based on the wide regional distribution and the dozens of Chagres-Bayano arc samples dated, this temporal gap is unlikely to be due to insufficient sampling. A temporal gap during the Chagres-Bayano arc magmatic episode is also supported by the work of Kesler et al. (1977), who determined K-Ar ages for amphibole and feldspar from 65 to 53 Ma on the Azuero peninsula (Fig. 2) and 62–51 Ma at Cerro Azul on the eastern boundary of the Chagres region. The K-Ar ages of Maury et al. (1995) extend the volcanic arc toward the east into the Darien region of Panama from 61 to 55 Ma (the Rio Morti area east of Lake Bayano in Fig. 2). These data fall within the age range observed for the Chagres region, and Kesler et al. (1977) reported K-Ar ages for feldspar and amphibole of 49–48 Ma for an in situ quartz diorite from the Rio Pito mineralized area farther east.

All of these observations above are in good agreement with the work of Recchi (1975) who postulated an E-W–trending volcanic arc between the Soná peninsula in Panama and northwestern Colombia during Late Cretaceous time (Fig. 1), which subsequently was offset by a sinistral motion along a northwest-trending fault zone that is located in the vicinity of the present-day Canal Zone. However, based on our high precision $^{40}Ar/^{39}Ar$ age data, we hold that magmatism of the Chagres-Bayano arc system was discontinuous in time and that the majority of arc magmatic products were generated in two main periods from 68 to 60 Ma and from 50 to 40 Ma.

TABLE 1. SUMMARY OF $^{39}Ar/^{40}Ar$ INCREMENTAL-HEATING EXPERIMENTS (FOR DETAILS, SEE COMPLETE Ar RESULTS)

						Plateau					Isochron		
Sample	Easting	Northing	Material	^{39}Ar (%)	MSWD	Age (Ma) ± 2σ		N	$^{40}Ar/^{36}Ar_i$ ± 2σ		MSWD	Age (Ma) ± 2σ	
Soná-Azuero arc													
PAN-05-008	546883	831171	Amphibole	100.0	0.49	**67.46**	**± 1.92**	7 of 7	293.5	± 4.8	0.46	67.94	± 2.25
PAN-05-017	540660	833605	Amphibole	100.0	0.56	72.34	± 2.50	10 of 10	296.1	± 1.1	0.47	71.68	± 2.77
			Amphibole	94.5	0.88	68.89	± 3.25	6 of 7	296.6	± 4.4	1.03	67.50	± 6.42
			Weighted mean plateau age:			**71.10**	**± 2.00**		*Mean Isochron age:*			71.00	± 2.50
Chagres-Bayano arc													
PAN-03-004*	675034	1027177	Amphibole	100.0	0.65	**61.49**	**± 2.32**	10 of 10	292.4	± 23.4	0.74	61.94	± 3.70
PAN-03-007*	681638	1020020	Amphibole	100.0	1.11	**49.38**	**± 1.04**	5 of 5	301.4	± 64.6	1.45	49.31	± 1.41
PAN-03-014*	680980	1045712	Amphibole	100.0	0.68	40.58	± 1.12	8 of 8	296.7	± 5.2	0.75	40.44	± 1.32
			Amphibole	100.0	0.77	42.54	± 1.20	12 of 12	299.2	± 8.5	0.76	42.14	± 1.54
			Weighted mean plateau age:			**41.56†**	**± 2.77**		*Mean Isochron age:*			41.20	± 1.00
PAN-03-022*	742621	1022253	Amphibole	100.0	0.17	68.52	± 5.02	10 of 10	297.9	± 12.4	0.13	67.15	± 8.69
			Amphibole h	100.0	1.24	64.90	± 4.15	9 of 9	294.2	± 10.2	1.41	65.21	± 4.76
			Weighted mean plateau age:			**66.40**	**± 3.20**		*Mean Isochron age:*			65.70	± 4.20
PAN-03-023*	740368	1022022	Amphibole	98.7	1.01	**65.85**	**± 2.88**	7 of 8	298.7	± 5.3	0.93	65.06	± 3.18
PAN-03-029*	696761	1032600	Amphibole	100.0	0.35	**47.15**	**± 1.44**	8 of 8	301.4	± 14.7	0.25	46.93	± 1.57
PAN-04-004*	684340	1035284	Amphibole	95.1	0.79	**49.49**	**± 1.01**	5 of 6	298.7	± 32.5	1.04	49.37	± 1.63
PAN-04-011*	705127	1026820	Amphibole	100.0	0.70	**47.18**	**± 1.29**	8 of 8	293.8	± 6.4	0.58	47.34	± 1.42
PAN-06-100	687479	1057551	Amphibole	99.1	1.27	64.58	± 2.24	8 of 9	314.0	± 20.9	0.89	62.49	± 3.15
			Amphibole	82.8	1.64	66.62	± 2.36	4 of 7	375.6	± 115.6	0.91	59.94	± 9.49
			Weighted mean plateau age:			**65.50**	**± 1.60**		*Mean Isochron age:*			62.20	± 2.90
PAN-06-103	686572	1049670	Amphibole	99.2	0.24	**44.75**	**± 1.43**	8 of 9	294.3	± 4.1	0.22	45.04	± 1.71
PAN-06-206	787121	1017837	Amphibole	100.0	0.37	**49.90**	**± 2.16**	8 of 8	296.5	± 2.5	0.34	49.53	± 2.39
PAN-06-210	763828	1017971	Amphibole	100.0	0.61	**46.92**	**± 3.55**	7 of 7	296.4	± 3.2	0.67	46.29	± 3.85
Cordilleran arc													
PAN-03-032*	561246	956056	Whole rock	95.2	1.63	14.68	± 0.45	12 of 13	295.0	± 5.8	1.79	14.72	± 0.64
			Whole rock	95.8	0.41	14.73	± 0.51	7 of 8	297.9	± 5.5	0.34	14.55	± 0.65
			Weighted mean plateau age:			**14.70**	**± 0.34**		*Mean Isochron age:*			14.64	± 0.46
PAN-05-056	644264	10000475	Plagioclase	84.6	0.37	**19.16**	**± 0.50**	6 of 7	297.2	± 2.1	0.29	18.40	± 1.07
PAN-06-023	342602	973594	Amphibole	100.0	0.84	**7.33**	**± 0.35**	9 of 9	294.5	± 4.6	0.94	7.35	± 0.36
PAN-06-041	412166	923412	Matrix	84.9	0.50	**14.17**	**± 0.42**	6 of 7	296.8	± 4.8	0.54	13.28	± 3.16
PAN-06-068	525602	936831	Amphibole	100.0	0.10	**6.78**	**± 0.14**	6 of 6	295.1	± 4.8	0.12	6.81	± 0.39
PAN-06-125	366791	968935	K-feldspar	96.2	1.05	**7.10**	**± 0.05**	6 of 7	300.5	± 7.8	0.88	7.06	± 0.08
PAN-06-131	366678	957373	Amphibole	100.0	0.14	**8.74**	**± 0.25**	6 of 6	295.9	± 1.2	0.04	8.67	± 0.31
PAN-06-185a	473894	935335	K-feldspar	100.0	0.29	8.62	± 0.10	6 of 6	295.5	± 1.5	0.36	8.62	± 0.22
			K-feldspar	100.0	0.74	8.68	± 0.12	6 of 6	293.5	± 4.1	0.70	8.81	± 0.29
			Weighted mean plateau age:			**8.65**	**± 0.08**		*Mean Isochron age:*			8.68	± 0.17
PAN-06-218	620728	952062	Plagioclase	100.0	0.52	**10.72**	**± 0.11**	7 of 7	297.0	± 6.9	0.59	10.70	± 0.16
Adakite suite													
PAN-05-047	515419	932671	Amphibole	100.0	0.99	**0.26**	**± 0.04**	7 of 7	297.9	± 6.6	1.08	0.23	± 0.08
PAN-05-049	515419	932671	Amphibole	100.0	0.76	**0.46**	**± 0.07**	6 of 6	302.3	± 12.7	0.65	0.34	± 0.21
PAN-06-006	308969	976393	Amphibole	92.5	0.33	**1.32**	**± 0.18**	5 of 6	294.7	± 5.0	0.39	1.45	± 0.78
PAN-06-010	311164	976475	Amphibole	100.0	1.06	**1.49**	**± 0.10**	6 of 6	290.7	± 13.5	0.21	1.53	± 0.16
PAN-06-014	312003	975064	Amphibole	100.0	0.23	**0.63**	**± 0.06**	6 of 6	296.1	± 5.0	0.28	0.62	± 0.09
PAN-06-043	415967	935660	Amphibole	100.0	0.71	**0.82**	**± 0.13**	5 of 5	297.8	± 11.1	0.95	0.78	± 0.25
PAN-06-044	415724	938624	Amphibole	100.0	0.28	**0.92**	**± 0.16**	5 of 5	299.0	± 6.8	0.03	0.82	± 0.26
PAN-06-073	535861	925254	Amphibole	100.0	0.96	**1.37**	**± 0.09**	6 of 6	296.8	± 10.5	1.18	1.34	± 0.24
PAN-06-136	324735	940222	Amphibole	99.7	0.49	**0.32**	**± 0.06**	5 of 6	296.7	± 4.2	0.55	0.28	± 0.13
PAN-06-166	340254	973213	Amphibole	99.4	0.25	**0.18**	**± 0.08**	6 of 7	295.5	± 2.9	0.31	0.18	± 0.12
PAN-06-168	337490	974820	Amphibole	92.8	0.73	**0.19**	**± 0.09**	4 of 6	299.2	± 16.5	0.99	0.13	± 0.15
PAN-06-176	326350	955330	Amphibole	100.0	0.48	**0.48**	**± 0.08**	6 of 6	295.5	± 5.9	0.60	0.48	± 0.15

Note: All ages calculated using the decay constants of Steiger and Jäger, 1977 ($\lambda_{40K} = 5.543 \times 10^{-10}$ yr^{-1}).
J-value calculated relative to 28.34 Ma for the Fish Canyon sanidine (Renne et al., 1998) unless noted otherwise.
*J-value calculated relative to 28.02 Ma for the Fish Canyon sanidine (Renne et al., 1998).
†Mean and 2× standard deviation reported for plateau age of this sample due to heterogeneity.
Age in **bold** is preferred. MSWD—mean square of weighted deviates.

Rocks of the Cordilleran arc suite underlying the El Valle and La Yeguada volcanic areas, scattered regions of the Cordillera de Panama, and domes from the forearc region (Fig. 2) range mostly in K-Ar ages from 22 to 7 Ma (de Boer et al., 1988, 1991; Defant et al., 1992; Drummond et al., 1995) with few exceptions (Fig. 5; Kesler et al., 1977; de Boer et al., 1995). Our new ages from the main Cordillera de Panama and the forearc regions (19.2 and 6.8 Ma) also fall within this range (Table 1), consistent with the majority of the K-Ar ages. We therefore argue that the main phase of magmatic activity of the Cordilleran arc occurred between 22 and 7 Ma. This phase was followed by a volcanic lull of 2 to 5 million years (Fig. 5B) after which only adakites were erupted in southern Costa Rica and western Panama. It is interesting to note that an older volcanic gap between 11 and 6 Ma was also observed in southern Costa Rica by MacMillan et al. (2004). These authors, however, noted intrusive activity during this time based on dating plutonic rocks that became exposed during strong uplift after the collision of the Cocos Ridge. Such significant uplift did not occur in western Panama, and thus intrusive rocks younger than 7 Ma may have remained concealed.

The heavy rare earth element (HREE)–depleted andesites and dacites of the Adakite suite were erupted only at isolated, geographically scattered volcanic centers in southern Costa Rica and west-central Panama over the past 3.5 million years

(de Boer et al., 1995; Johnston and Thorkelson, 1997; Abratis and Wörner, 2001; and new data from this study; Table 1). These adakitic rocks are associated with stratovolcanoes at El Valle, La Yeguada, and Barú, and occur as remnants of dacitic ignimbrites that span the Panama–Costa Rica border (Defant and Drummond, 1990; Defant et al., 1991a, 1991b, 1992).

Trace Element Geochemistry

The trace element compositions of the rocks analyzed in this study are compiled in the full data table (see footnote 1). Mantle-normalized trace element patterns are shown in Figure 6, which displays clear differences in trace element patterns for the different age groups with respect to levels of incompatible element enrichment and concentrations of HFSE.

Caribbean large igneous province trace element patterns in Figure 6 are almost horizontal, with only a few, unsystematic variations observed for the fluid-mobile elements such as Ba, K, Pb, and Sr. These variations are probably a consequence of secondary, low-temperature hydrothermal alteration. Accreted OIB shows a clear enrichment in the more incompatible elements and low rare earth element patterns to the right of Sm (HREE) concentrations relative to Caribbean large igneous province and primitive mantle (Fig. 6). This pattern indicates an intraplate mantle source, an interpretation that is consistent with the ideas of Alvarado et al. (1992) and Hoernle et al. (2002), who described a set of 70–20 Ma accreted terranes from Costa Rica that have this same trace element signature. These were interpreted as seamounts from the Galápagos hotspot track that were accreted to the Central American arc (Fig. 1). The Soná-Azuero arc samples show a clear subduction-related volcanic arc trace element signature that is characterized by depletion in Nb and Ta and enrichment of fluid-mobile elements such as Ba, K, Pb, and Sr. These are rare rocks within the Soná and Azuero peninsulas (Figs. 1 and 2) and provide important insights into the earliest evolution of the volcanic arc in this region (Buchs et al., 2007). Unfortunately, we have no information about structural relations relative to the other Caribbean large igneous province rocks due to their very limited exposure. The new

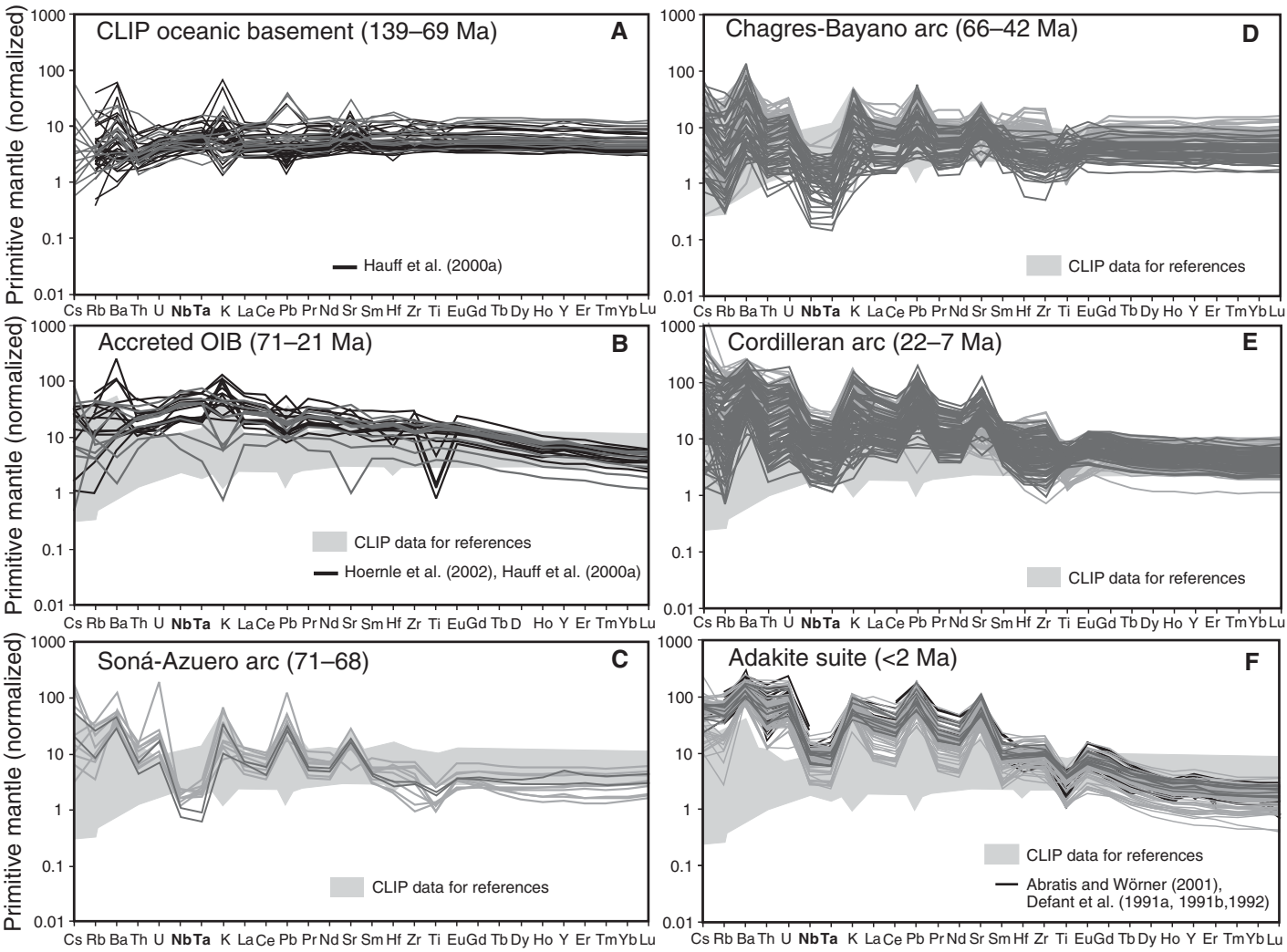

Figure 6. Trace element patterns, normalized to primitive mantle (Sun and McDonough, 1989), for igneous rocks from central and western Panama. Elements are plotted according to their decreasing incompatibility from left to right. Dark gray denote samples with SiO_2 <57 wt%, whereas pale gray indicate samples with SiO_2 >57 wt%. The light-gray field shows the Caribbean large igneous province data for reference. Literature data from the sources cited in the text are shown in black lines for comparison. CLIP—Caribbean large igneous province; OIB—ocean island basalt.

$^{40}Ar/^{39}Ar$ ages for Soná-Azuero arc rocks range from 68 to 71 Ma and, thus, are slightly older than those observed for the Chagres-Bayano arc rocks of the Chagres region (see below).

Most rocks of the Chagres-Bayano arc were sampled in the Chagres region northeast of the Panama Canal (Fig. 2) and in the Bayano area to the east. The large geochronological data set shown in Figure 5 and, in particular, the new $^{40}Ar/^{39}Ar$ ages for the Chagres region show that voluminous subduction magmatism in this region started somewhat earlier at 66 Ma, slightly later than in the Soná and Azuero areas where arc magmatism is first recorded at 71 Ma, and lasted until 42 Ma. Most Chagres-Bayano arc samples are characterized by horizontal trace element patterns to the right of Sm similar to Caribbean large igneous province samples, although a few rocks are relatively enriched, whereas others are relatively depleted by comparison. The most obvious geochemical feature of this group is the large variation in Nb and Ta and for some samples a very strong depletion in these elements. Some of the samples are even below primitive mantle values in Nb and Ta. Because Nb and Ta are not affected by fluid addition, this implies that the mantle source region at this time was heterogeneous and subject to large variations in incompatible element composition prior to fluid enrichment. An alternative view would attribute this feature to involvement of variable amounts of subducted sediments, or fluids derived therefrom, in their source (see discussion below). We have insufficient data to test whether there are systematic compositional changes with time in this group or if there might be a compositional trend from tholeiitic to calc-alkaline rocks as the arc matured. However, there is a clear compositional difference between the Soná-Azuero arc and Chagres-Bayano arc rocks (71–42 Ma) and Caribbean large igneous province basement rocks that were erupted before 69 Ma (Hoernle et al., 2004).

Compared to the Chagres-Bayano arc, samples of the Cordilleran arc exhibit a slightly narrower range in Nb and Ta concentrations. Only very few samples from this phase of magmatism have depleted trace element patterns, which is typical of many of the arc magmas erupted earlier in the development of the Panama volcanic arc system (Figs. 6–8). Based on trace element ratios and patterns (Figs. 6–8), we conclude that the change from a depleted tholeiitic magma source indicative of the early stage of arc magmatism to a more mature, less depleted magma source must have taken place at the beginning of the Cordilleran arc magmatic episode at ~22 Ma. This change also involved a transition to a more homogeneous magma source with time.

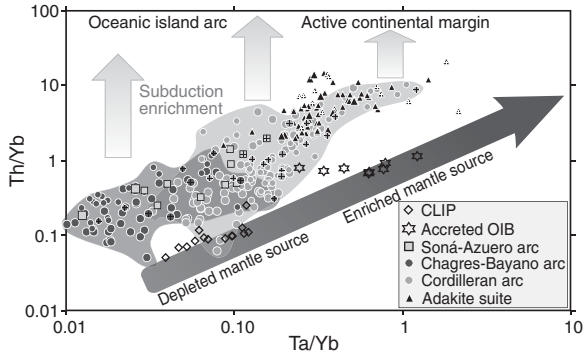

Figure 7. Plot of Ta/Yb versus Th/Yb for magmatic rocks from central and western Panama. This diagram can be used to recognize arc magmas generated via subduction and fluid enrichment of a depleted to enriched mantle sources. Large symbols denote samples with <57 wt% SiO_2, whereas small symbols indicate samples with >57 wt% SiO_2. $^{40}Ar/^{39}Ar$ dated samples are denoted with crosses. CLIP—Caribbean large igneous province; OIB—ocean island basalt.

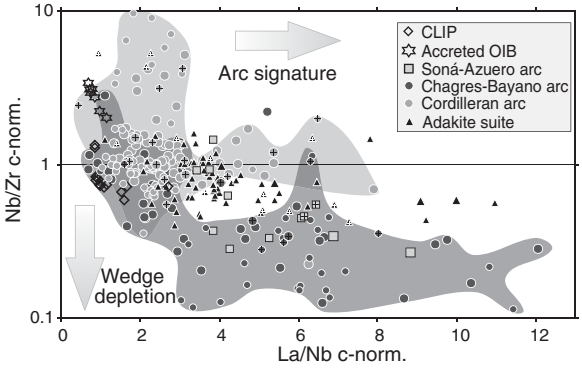

Figure 8. Plot of chondrite normalized ratios of La/Nb versus Nb/Zr showing the different effects of wedge depletion and arc signature for the different arc groups. Large symbols denote samples with <57 wt% SiO_2. $^{40}Ar/^{39}Ar$ dated samples denoted with crosses.

The Adakite suite forms a separate group that is characterized by steep REE patterns from Sm to Yb (Fig. 6), which is diagnostic of residual garnet in the magma source. Our samples of this group are all younger than 2 Ma, indicating a gap in magmatism of a few million years between the cessation of the Cordilleran arc stage of magmatism and the onset of the Adakite suite phase. There are two models for genesis of the Panama–Costa Rican adakites. Johnston and Thorkelson (1997) argue that a slab window formed due to subduction of the Panama spreading center and that Cocos plate mid-ocean ridge basalt (MORB) then melted to form adakitic magmas. By contrast, Abratis and Wörner (2001) consider that Cocos MORB is not a viable source for the adakites and instead, based on Pb isotope evidence, favor melting of the leading edge of the Cocos ridge (Fig. 1) after its collision with the Chortis block and consequent slab window formation. In any case, the magma source for the Adakite suite stage of Panamanian magmatism is significantly different from that which produced the magmas during the earlier Soná-Azuero arc, Chagres-Bayano arc, and Cordilleran arc stages.

The plot of Ta/Yb versus Th/Yb in Figure 7 illustrates the effect of slab enrichment on depleted mantle source regions with low ratios of Th/Yb and Ta/Yb (i.e., MORB-source mantle) to mantle sources enriched in both Th and Ta (e.g., OIB-source mantle). Magmas produced by subduction-related arc magmatism in which enrichment of a depleted mantle source occurs by the introduction of LILE-enriched fluids and sediments, are differentiated in Figure 7 by their enrichment in Th but not Ta, i.e., higher Th/Yb ratio at constant Ta/Yb ratio.

The Caribbean large igneous province basement rocks fall largely within the depleted mantle field in Figure 7. By contrast, accreted OIB samples have higher Th/Yb and Ta/Yb ratios that are indicative of derivation from an enriched mantle source, whereas the Soná-Azuero arc samples have higher Th/Yb ratios only that are suggestive of fluid enrichment of a depleted mantle source. Overall, the Chagres-Bayano arc, Cordilleran arc, and Adakite suite samples in Figure 7 define a trend that is parallel to the mantle trend with higher Th/Yb ratios. Samples of the Soná-Azuero arc group form a field contained within the low Ta/Yb portion of the broad field defined by the Chagres-Bayano arc rocks.

This situation is not unexpected, as both groups are considered to have been derived from a depleted mantle wedge source (see above). As demonstrated by their trace element patterns (Fig. 6), the Chagres-Bayano arc reflects a fluid-modified but variable depleted mantle source, as documented by the more than one orders of magnitude range observed in both Th/Yb and Ta/Yb ratios. By comparison, the majority of rocks of the Cordilleran arc require a more enriched magma source composition that overlaps the high-Ta/Yb end of the Chagres-Bayano arc field and extends into high values of the Adakite suite field. The Cordilleran arc is in the same range as the Chagres-Bayano arc in terms of degree of homogeneity and fluid modification of the mantle source. The Adakite suite exhibits the highest Ta/Yb and Th/Yb ratios, which is interpreted to reflect the strong subduction enrichment of an already enriched mantle source.

The arc signature is strongest for the Adakite suite and Chagres-Bayano arc samples (Fig. 8). For the Chagres-Bayano arc this may be mainly due to the depleted source composition, which even for a small amount of arc fluids produces a large effect. The Cordilleran arc samples display less of an arc signature, and most are clearly more enriched than Chagres-Bayano arc and Soná-Azuero arc samples. The Soná-Azuero arc is intermediate between the Chagres-Bayano arc and the Cordilleran arc in terms of wedge depletion and arc signature.

The trace element patterns of Figure 6 and ratios of Figure 7 and 8 document a systematic temporal evolution in magma composition beginning in Cretaceous time that continues to the present. We interpret this change in mantle source composition over more than 100 million years to be related to tectonic rearrangements in a developing complex arc setting through time (see below).

Oxygen Isotope Geochemistry

The object of the O-isotope portion of the study was to determine the primary magmatic $\delta^{18}O$ values for a subset of 56 of the Panamanian intrusive and volcanic rocks using theoretical and experimental mineral-mineral and mineral-melt isotopic fractionations and thereby establish the O-isotope character of the source region from which their parental melts originated. The samples analyzed span a wide range in bulk composition from 46% to 77% SiO_2. As a consequence of their age and complex geological history, the samples were subjected to varying degrees of post-crystallization alteration, and several samples display visible alteration in hand specimen or thin section. Because of concern about the geochemical integrity of some samples, it was not appropriate to determine the O-isotope composition of whole rocks. Instead, $^{18}O/^{16}O$ ratios were measured for 87 mineral separates that appeared to be entirely free of alteration under a binocular microscope that were obtained by hand-picking from seven intrusive rocks, one magmatic segregation vein, and phenocrysts from 47 volcanic samples. A particular focus was on the mafic minerals amphibole and clinopyroxene, but plagioclase, which is more susceptible to the effects of post-crystallization, O-isotopic modification, was included where present, and the glass matrix of three volcanic rocks was also sampled. Measured $^{18}O/^{16}O$ ratios are reported in Table 2 in the familiar "δ" notation [$\delta^{18}O_{(‰)} = (^{18}O/^{16}O_{sample}/^{18}O/^{16}O_{standard} - 1) \times 1000$] relative to the VSMOW, together $\delta^{18}O$ values estimated for equilibrium magmas at high temperature that were calculated following the procedure of Bindeman et al. (2004). From the analysis below, magmatic $\delta^{18}O$ values were estimated for 41of the 56 rocks of this study, 15 of which were based on $^{18}O/^{16}O$ ratios of multiple minerals.

Table 2 presents $^{18}O/^{16}O$ ratio measurements for 47 amphibole, 11 clinopyroxene, and 29 plagioclase separates. The distribution of these $\delta^{18}O$ values is shown in histogram form in Figure 9, and their ranges for the four groups sampled are presented in Table 3. For the Panama suite as a whole, $\delta^{18}O_{am}$ = 3.6‰ to 6.9‰, $\delta^{18}O_{cpx}$ = 4.9‰ to 6.6‰, and $\delta^{18}O_{fsp}$ = 3.9‰ to 10.9‰. The range of O-isotope variation observed for feldspar (7.0‰) is much larger than that for amphibole (3.3‰), which in turn is about twice that recorded for clinopyroxene (1.7‰), which was only separated from the adakite lavas. The sections that follow discuss the extent to which this O-isotope data can be used to estimate magmatic $^{18}O/^{16}O$ for the parental magmas of the Panamanian igneous rocks.

From studies of peridotite xenoliths (Ionov et al., 1994; Mattey et al., 1994) and a wide variety of volcanic rocks (Eiler et al., 1996, 1997, 2000; Bindeman et al., 2004, 2005), it is known that normal basaltic melts derived from hydrous melting of the subducting mantle wedge in convergent plate margin settings should have $^{18}O/^{16}O$ ratios in the range of $\delta^{18}O = 5.8 \pm 0.2$‰ and, as demonstrated by Matsuhisa (1979), Harmon and Gerbe (1992), and Bindeman et al. (2004), derivative high-Si dacitic to rhyolitic melts produced solely by closed-system crystal fraction should have elevated $\delta^{18}O$ values that can range up to a maximum of ~7‰. Rare instances of young subduction-zone volcanic rocks containing olivine with $\delta^{18}O$ up to 7.1‰, implying melt $\delta^{18}O$ values of up to ~8‰, have been documented for Kamchatka (Dorendorf et al., 2000; Bindeman et al., 2004) and for a variety of adakites from Panama (Abratis, 1998; Bindeman et al., 2005) and various other circum-Pacific localities by Bindeman et al. (2005).

Because most rocks and fluids contain similar concentrations of oxygen, the O-isotope composition of an igneous rock can be used both as a screening tool for evaluating effects of secondary alteration and, if high-temperature equilibrium O-isotope systematics are observed, variations in $^{18}O/^{16}O$ ratios also can be used as an additional petrogenetic indicator and guide to magma source character and process because oxygen isotopes provide geochemical information that is complementary to that derived from trace elements and radiogenic isotopes. To ascertain if measured $^{18}O/^{16}O$ ratios are pristine and have not been affected by secondary modification, measured $\delta^{18}O$ values can be evaluated based on equilibrium mineral-mineral and mineral-melt O-isotope fractionations expected on the basis of theoretical considerations (Kieffer, 1982; Zheng, 1991, 1997; Zhao and Zheng, 2003; Bindeman et al., 2004) or laboratory experiments (Matthews et al., 1983; Chiba et al., 1989; Chacko et al., 2001). The ^{18}O content of a bulk rock, particularly fine-grained magmatic rocks or subvolcanic intrusives, can be readily modified by water-rock interactions both at high and low temperature (see, e.g., Gregory et al., 1989). Radiogenic isotopes systems, particularly Sr, may also be affected by secondary alteration, if sufficiently intense. Most natural waters are ^{18}O deficient compared to magmatic silicate rocks. Thus, isotopic exchange as a consequence of water-rock interaction at high temperatures, where fractionation coefficients are small, will result in a lowering of rock $\delta^{18}O$ values. By contrast, weathering and alteration in the near-surface environment will be characterized by strong ^{18}O enrichment because fractionation factors are large at low temperatures. A variety of studies have shown that most Tertiary and older volcanic rocks have elevated $^{18}O/^{16}O$ ratios as a consequence of hydration and weathering at Earth's surface (Muehlenbachs and Clayton, 1972; Taylor et al., 1984; Cerling et al., 1985; Harmon et al., 1987). Silicic glass and feldspar are the phases most susceptible to secondary alteration, but even minerals like amphibole and pyroxene can have their $^{18}O/^{16}O$ ratios modified through high degrees of water-rock interaction particularly at elevated temperature. Two approaches can be taken to ascertain whether measured $^{18}O/^{16}O$ ratios are pristine or have been affected by secondary modification.

Based on a careful screening of our data using predicted equilibrium fractionation, 56 of the 87 mineral separates analyzed (Table 2) have $\delta^{18}O$ values that are considered to be representative of

TABLE 2. OXYGEN-ISOTOPE COMPOSITION OF MINERALS AND $\delta^{18}O_{magma}$ VALUES CALCULATED FOLLOWING THE PROCEDURE OF BINDEMAN ET AL. (2004)

Sample	Rock type	$\delta^{18}O_{amp}$	$\delta^{18}O_{cpx}$	$\delta^{18}O_{plag}$	SiO_2 (wt%)	MgO (wt%)	Calculated $\delta^{18}O$ in melt[§]
Soná-Azuero arc							
PAN-05-007	Andesite	6.6	N.D.	N.D.	62.74	7.43	N.D.
PAN-05-008	Dacite	5.9	N.D.	7.8	63.12	6.85	7.0
PAN-05-017	Dacite	5.3	N.D.	8.3	67.82	4.28	6.7
Chagres-Bayano arc							
PAN-03-004	Microdiorite	4.5	N.D.	7.2	54.99	4.63	N.D.
PAN-03-007	Gabbro	5.4	N.D.	4.7	49.49	7.20	5.7
PAN-03-014	Andesite	5.9	N.D.	7	62.34	2.40	7.10 ± 0.14
PAN-03-022	Granodiorite	3.6	N.D.	9.1	61.97	3.52	N.D.
PAN-03-023	Andesite	6.4	N.D.	9.9	62.96	2.68	N.D.
PAN-03-029	Basaltic andesite	5.5	N.D.	6	54.05	6.62	6.05 ± 0.07
PAN-04-004	Andesite	5.4	N.D.	7.4	59.42	3.31	6.3
PAN-04-011	Granodiorite	4.9	N.D.	7.4	61.57	3.05	5.9
PAN-06-100	Andesite	3.8	N.D.	N.D.	57.17	6.56	N.D.
PAN-06-103	Andesite	4.7	N.D.	N.D.	56.99	3.71	N.D.
PAN-06-104	Segregation	3.9	N.D.	N.D.	53.73	3.33	N.D.
PAN-06-206	Granodiorite	4.7	N.D.	N.D.	63.37	3.01	5.8
PAN-06-210	Andesite	5	N.D.	N.D.	61.07	3.54	6.0
Cordilleran arc							
PAN-03-032	Basaltic andesite	6	N.D.	10.9	56.53	4.90	N.D.
PAN-05-031	Andesite	N.D.	N.D.	5.8	59.78	2.56	6.0
PAN-05-056	Basaltic andesite	N.D.	N.D.	6	53.11	4.33	6.0
PAN-05-066	Basaltic andesite	N.D.	N.D.	6.8	52.77	5.18	N.D.
PAN-06-023	Diorite	4.6	N.D.	N.D.	46.02	4.15	N.D.
PAN-06-068	Andesite	4.4	N.D.	N.D.	60.78	3.55	N.D.
PAN-06-125	Rhyolite	N.D.	N.D.	7.1	77.17	0.23	N.D.
PAN-06-131	Dacite	4.9	N.D.	N.D.	64.10	1.85	6.1
PAN-06-185a	Granite	N.D.	N.D.	3.9	67.30	1.45	N.D.
PAN-06-218	Rhyolite	N.D.	N.D.	5.9	74.39	0.32	6.5
PAN-06-219	Dacite	5.2	N.D.	N.D.	64.28	1.91	6.4
Adakite suite							
PAN-05-047	Dacite	5.5	N.D.	7.6	69.68	0.92	7.50 ± 0.76
PAN-05-049	Dacite	5.5	N.D.	6.8	70.57	0.76	7.20 ± 0.14
PAN-06-006	Andesite	5.1	N.D.	N.D.	59.93	3.33	6.0
PAN-06-010	Dacite	5.3	N.D.	N.D.	63.50	2.67	6.5
PAN-06-014	Andesite	4.9	N.D.	N.D.	57.21	3.30	5.7
PAN-06-043	Dacite	6.9	N.D.	N.D.	66.96	1.31	N.D.
PAN-06-044	Dacite	3.9	N.D.	N.D.	67.22	1.31	N.D.
PAN-06-073	Dacite	4.8	N.D.	N.D.	65.60	1.03	6.1
PAN-06-136	Andesite	5.1	N.D.	N.D.	60.32	2.93	6.1
PAN-06-137a	Andesite	5.9	6.4	7.5	60.76	3.32	7.33 ± 0.40
PAN-06-137b	Andesite	4.5	N.D.	7.3	60.46	3.46	6.5 ± 1.41
PAN-06-137d	Andesite	5.8	6.6	7.5	60.54	3.41	7.37 ± 0.49
PAN-06-138b	Dacite	5.5	N.D.	6.4	65.48	2.02	6.75 ± 0.07
PAN-06-140	Andesite	5	N.D.	N.D.	58.23	4.74	5.8
PAN-06-141	Basaltic andesite	N.D.	5.4	N.D.	55.99	6.22	6.1
PAN-06-161	Andesite	5.5	N.D.	N.D.	60.82	3.24	6.5
PAN-06-165	Andesite	5.3	4.9	N.D.	61.13	3.00	6.1 ± 0.28
PAN-06-166	Andesite	5.2	5.5	7.3	58.84	3.54	6.65 ± 0.68
PAN-06-168	Andesite	5.2	N.D.	N.D.	60.87	3.35	6.2
PAN-06-169	Andesite	5.6	N.D.	N.D.	60.67	3.43	6.6
PAN-06-170	Andesite	5.7	N.D.	N.D.	59.88	3.58	6.6
PAN-06-173	Andesite	5.2	5.4	N.D.	59.46	3.33	6.20 ± 0.14
PAN-06-174	Andesite	N.D.	5.6	N.D.	57.55	4.13	6.4
PAN-06-175	Andesite	5	5.2	6.4	58.39	4.65	6.10 ± 0.36
PAN-06-176	Andesite	5.2	5.8	7.5	58.89	3.41	6.86 ± 0.70
PAN-06-177	Andesite	4.7	5.1	6.1	59.35	3.44	6.00 ± 0.35
PAN-06-179	Andesite	4.9	N.D.	6.3	61.13	3.10	6.35 ± 0.21
PAN-06-183	Andesite	4.6	N.D.	6.5	61.38	3.00	6.15 ± 0.78
PAN-06-184	Andesite	N.D.	6.3	N.D.	59.75	3.39	7.2

[§]Magma $^{18}O/^{16}O$ ratios were estimated only for those instances where expected high-temperature fractions were observed for mineral pairs or where minerals with measured $\delta^{18}O$ values that fall within the range expected for the unaltered host rock composition. Averages and standard deviation values are given for multiple estimates of $\delta^{18}O_{magma}$ derived from two or three measured mineral $\delta^{18}O$ values.

Note: Matrix glass was obtained from three Cordilleran arc volcanic rocks, basaltic andesite PAN-03-032, dacite PAN-06-041, and rhyolite PAN-06-218. Respective measured $\delta^{18}O$ values for these samples are 5.9‰, 8.4‰, and 12.9‰.

the magmas from which the minerals crystallized based upon measured $^{18}O/^{16}O$ ratios and mineral-pair fractionations. A group of 31 minerals are considered to have anomalously low or high $^{18}O/^{16}O$ ratios that indicate post-crystallization modification (Fig. 10). As expected, feldspar is the mineral most affected by post-crystallization alteration, with only five of the Soná-Azuero arc, Chagres-Bayano arc, and Cordilleran arc plagioclase separates having O-isotope ratios that fall within the $\delta^{18}O$ range of 5.6‰ to 7.0‰ expected for normal subduction zone magmatic rocks. The other 13 feldspars, independent of their age group or rock type, have lower or higher $\delta^{18}O_{pl}$ values that are outside this range and indicative of post-crystallization secondary modification. Some of these feldspars have a cloudy appearance in thin section, consistent with this interpretation. Two samples (gabbro PAN-03-007 with $\delta^{18}O_{pl} = 4.7‰$ and granite PAN-06-185a with $\delta^{18}O_{pl} = 3.9‰$) have $\delta^{18}O_{pl}$ values below 5.5‰ that are indicative of high-temperature subsolidus hydrothermal alteration. Four other samples (dacite PAN-05-017 with $\delta^{18}O_{pl} = 8.3‰$, granodiorite PAN-03-022 with $\delta^{18}O_{pl} = 9.1‰$, andesite PAN-03-023 with $\delta^{18}O_{pl} = 9.9‰$, and basaltic andesite PAN-03-032 with $\delta^{18}O_{pl} = 10.9‰$) are strongly ^{18}O enriched with $\delta^{18}O$ values elevated above 8‰ that have been produced by secondary alteration at low temperature. Twelve samples have $\delta^{18}O_{pl}$ values in the intermediate range from between 7‰ and 8‰ that are more difficult to interpret. However, based upon either (1) a normal $\delta^{18}O$ value for coexisting amphibole or (2) a $\delta^{18}O_{pl}$ value higher than expected for the bulk composition of the host rock, these samples are considered to have not fully retained the original O-isotope signature so that magmatic $\delta^{18}O$ values were not estimated for these samples from the measured feldspar $^{18}O/^{16}O$ ratios.

Matrix glass samples were analyzed for three Cordilleran arc volcanic rocks. Two of these samples, one from dacite PAN-06-041 with $\delta^{18}O_{gl} = 8.4‰$ and the other from PAN-06-218 with $\delta^{18}O_{gl} = 12.9‰$, exhibit strong ^{18}O enrichment as a consequence of low-temperature hydration. This is not surprising given the Miocene age and silicic composition of these glasses. The third glass sample, with $\delta^{18}O_{gl} = 5.9‰$, comes from basaltic andesite PAN-03-032. This sample contains strongly ^{18}O-enriched feldspar with $\delta^{18}O_{pl} = 10.9‰$ that could only have been produced by post-crystallization alteration at low temperature. The $\delta^{18}O_{am} = 6.0‰$, for the amphibole from this rock also has elevated relative to the normal basaltic-andesitic range, but to a far lesser extent than its companion feldspar. Thus, the O-isotopic composition of the glass, although appearing reasonable for

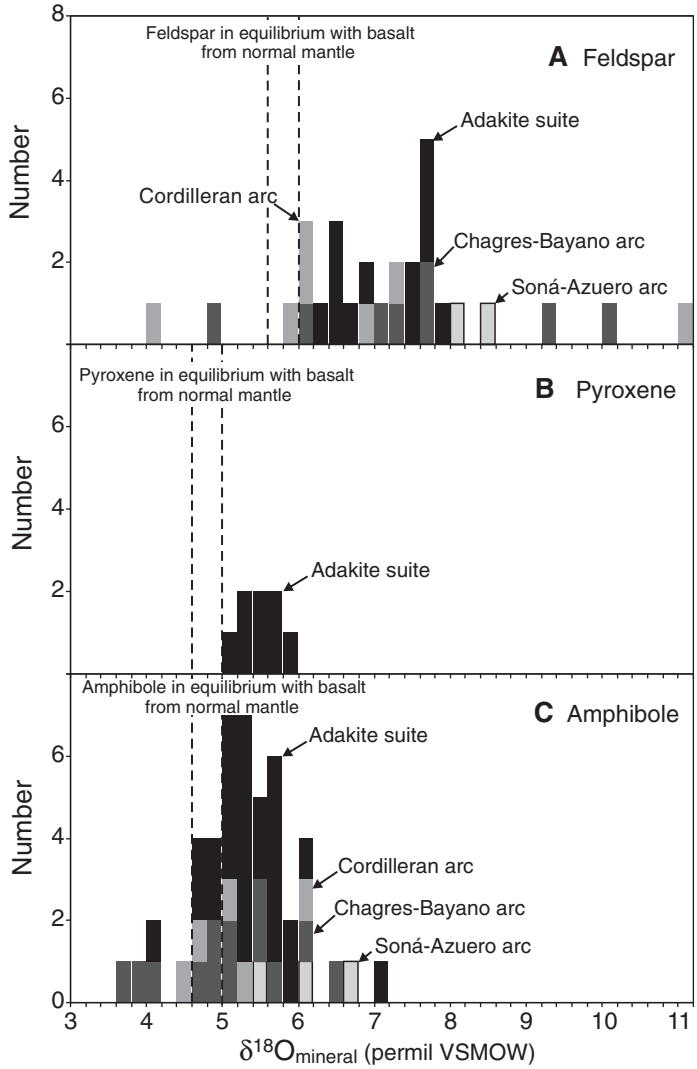

Figure 9. Histogram of $\delta^{18}O$ values illustrating the O-isotope variation in (A) feldspar, (B) pyroxene, and (C) amphibole for Panamanian igneous rocks. The dashed lines denote the field for the mineral in equilibrium with parental basalts generated within the mantle wedge in convergent plate margin subduction zone settings, from 5.6‰ to 6.0‰ for feldspar and 4.6‰ to 5.0‰ for pyroxene and amphibole. A process of magmatic evolution through only closed-system fractionation will produce evolved rhyodacitic magmas from a basaltic parent magma that are enriched in ^{18}O by ≤1‰ (Matsuhisa, 1979; Harmon and Gerbe, 1992; Bindeman et al., 2005). Feldspar crystallized under equilibrium from highly evolved rhyodacitic melts will be enriched in ^{18}O by ~0.4‰ as compared with ~1.5‰ for pyroxene and amphibole. VSMOW—Vienna standard mean ocean water.

such an arc lava with $\delta^{18}O$ = 5.9‰, must be considered suspect.

In Figure 10, $^{87}Sr/^{86}Sr$ ratios are plotted versus $\delta^{18}O$ for amphibole and pyroxene (A) and feldspar (B). The field (A) in each plot denotes the field for the mineral in equilibrium with normal arc parental basalt magmas having $^{87}Sr/^{86}Sr$ = 0.7032–0.7034 and $\delta^{18}O$ = 5.6‰–6.0‰. The area (B) above the mantle magma field, bounded by the light-gray lines in each plot that extends to just above $^{87}Sr/^{86}Sr$ = 0.7042 denotes mantle source heterogeneity that produces ^{87}Sr-enriched basaltic magmas with normal $\delta^{18}O$ values. The introduction of seawater-derived fluids into the magma source also can elevate the $^{87}Sr/^{86}Sr$ ratio without affecting O-, Nd-, or Pb-isotope ratios. The two Adakite suite samples with the highest $^{87}Sr/^{86}Sr$ ratios (PAN-06-073 and PAN-06-165) have a likely source from the subducted oceanic basalt that had been affected by such seawater alteration. The area (C) to the right in each figure, indicated by gray box, denotes the ^{18}O enrichment possible through closed system fractional crystallization from basalt to rhyodacitic compositions. Rhyolite PAN-06-218 with a feldspar $\delta^{18}O$ value of 5.9‰ can be explained in this way. The different arrows indicate the sense of $^{87}Sr/^{86}Sr$–$\delta^{18}O$ trends for a process that can affect observed rock and mineral isotopic compositions. Combined assimilation-fractional crystallization (1) of parental magmas generate both ^{87}Sr- and ^{18}O-enriched phenocrysts in evolved andesite-rhyolite magmas. Chagres-Bayano arc andesite PAN-03-023 with $\delta^{18}O_{magma}$ = 7.10 ± 0.14‰ was likely a product of such an AFC (assimilation, fractionation, and crystallisation) process. Subsolidus high-temperature, seawater-rock interaction (2) with subvolcanic intrusives, or assimilation of such submarine hydrothermally altered crust, will result in concomitant ^{18}O depletion and ^{87}Sr enrichment. By contrast, subsolidus high-temperature interaction with meteoric hydrothermal water (3) will result in ^{18}O depletion but not affect $^{87}Sr/^{86}Sr$ ratios, whereas low-temperature alteration (4) will produce ^{18}O enrichment and not affect Sr-isotope composition. The two circles in the figures bound samples that have had their isotopic compositions modified by secondary processes. It can be seen from Table 2 and Figure 10 that some samples characterized by O-isotope disequilibrium have been affected by high-temperature alteration (e.g., granite PAN-06-185a with $\delta^{18}O_{pl}$ = 3.9‰), whereas others have been subjected to low-temperature alteration processes (e.g., basaltic andesite PAN-03-032 with $\delta^{18}O_{pl}$ = 10.9‰).

About half of the Soná-Azuero arc, Chagres-Bayano arc, and Cordilleran arc amphiboles O-isotope compositions are consistent with a mantle derivation of their host magmas. Clearly, the amphibole in granodiorite PAN-03-022, with an anomalously low $\delta^{18}O_{am}$ value of 3.6‰, has been affected by subsolidus water-rock interaction at high temperature, but to a lesser extent than the corresponding feldspar from the same rock. Samples PAN-06-100, PAN-06-044, and PAN-06-104 have similarly low $\delta^{18}O_{am}$ values of 3.8‰ and 3.9‰ that also document extensive subsolidus hydrothermal alteration of these rocks. The same is likely the case for three other samples: andesite PAN-06-068, with $\delta^{18}O_{am}$

TABLE 3. RANGES OF $\delta^{18}O$ VARIATION FOR PANAMANIAN IGNEOUS ROCKS

	No.	$\delta^{18}O_{amphibole}$	No.	$\delta^{18}O_{clinopyroxene}$	No.	$\delta^{18}O_{plagioclase}$	No.	$\delta^{18}O_{glass}$
Soná-Azuero arc	3	5.3 to 6.6		N.D.	2	7.8 to 8.3		N.D.
Chagres-Bayano arc	13	3.6 to 6.4		N.D.	8	4.7 to 9.9		N.D.
Cordilleran arc	5	4.4 to 6.0		N.D.	7	3.9 to 10.9	3	5.9 to 12.9
Adakite suite	26	3.9 to 6.9	11	4.9 to 6.6	12	6.1 to 7.5		N.D.

= 4.4‰, and both microdiorite PAN-03-004 and granodiorite PAN-04-011, with respective $\delta^{18}O_{am}$ values of 4.4‰ and 4.9‰ and elevated feldspar $\delta^{18}O$ values >7‰. The degree of secondary alteration is lower for these rocks than for PAN-03-022.

The amphibole $\delta^{18}O$ value of 6.6‰ for Soná-Azuero arc andesite PAN-05-007 indicates that this sample has suffered a significant degree of low-temperature alteration and ^{18}O enrichment. The large $\Delta_{pl\text{-}am}$ values of +1.9‰ and +3.0‰ for the two Soná-Azuero arc dacites, PAN-05-008 and PAN-05-01, indicate that the O-isotope composition is not pristine. With respective amphibole and feldspar $\delta^{18}O$ values of 5.9‰ and 7.8‰ for PAN-05-008 and 5.3‰ and 8.3‰ for PAN-05-017, this alteration appears to have been of sufficiently low water-rock ratio that amphibole $^{18}O/^{16}O$ ratios were retained intact, while the feldspar $^{18}O/^{16}O$ ratios were elevated ~1‰–2‰ as a consequence of low-temperature alteration. The magmatic $\delta^{18}O$ values estimated from the amphibole $^{18}O/^{16}O$ ratios for these two compositionally evolved lavas are 6.7‰ and 7.0‰, respectively.

For the Chagres-Bayano arc, six samples have O-isotope systematics that yield reliable estimates of magmatic O-isotope composition. With respective $\delta^{18}O_{am}$ and $\delta^{18}O_{pl}$ values of 5.5‰ and 6.0‰, and a $\delta^{18}O_{pl\text{-}am}$ value of +0.5‰, basaltic andesite PAN-03-029 had a parental magma $\delta^{18}O$ value of 6.05 ± 0.07‰. Very slightly lower magma $\delta^{18}O$ values of 5.7‰ and 5.9‰ are estimated for gabbro PAN-03-007 and granodiorite PAN-04-011 on the basis of their amphibole $^{18}O/^{16}O$ ratios. Three compositionally evolved Chagres-Bayano arc andesites (PAN-03-023, PAN-04-004, and PAN-06-210 with SiO_2 contents between 59 wt% and 62 wt%) have $\delta^{18}O_{magma}$ values ranging from 6.0 to 7.10 ± 0.14‰. The feldspar $^{18}O/^{16}O$ ratios for all Chagres-Bayano arc samples except basaltic andesite PAN-03-029 have been elevated by low-temperature alteration.

The only Cordilleran arc sample for which it was possible to separate both amphibole and feldspar is basaltic andesite PAN-03-032. With respective amphibole and plagioclase $\delta^{18}O$ values of 6.0‰ and 10.9‰, and a $\Delta\delta^{18}O_{pl\text{-}amp}$ value of +4.9‰, PAN-03-032 documents a significant degree of isotopic modification as a result of low-temperature secondary alteration. For the ten other Cordilleran arc samples, either amphibole or feldspar was analyzed. Two volcanic rocks also exhibit a modest level of $^{18}O_{pl}$ = 6.8‰ and rhyolite PAN-06-125 with $\delta^{18}O_{pl}$ = 7.1‰. By contrast, two samples from Cordilleran arc intrusive rocks and one volcanic sample have been affected by subsolidus water-rock interaction at elevated temperature, diorite PAN-06-023 with $\delta^{18}O_{am}$ = 4.6‰, andesite PAN-06-068 with $\delta^{18}O_{am}$ = 4.4‰, and granite PAN-06-185 with $\delta^{18}O_{am}$ = 3.9‰. Magmatic $\delta^{18}O$ values falling within the narrow range from 6.0‰ to 6.5‰ could be estimated for five Cordilleran arc samples: basaltic andesite PAN-05-56 with $\delta^{18}O_{pl}$ = 6.0‰, andesite PAN-05-031 with $\delta^{18}O_{pl}$ = 5.8‰, dacite PAN-06-131 with $\delta^{18}O_{am}$ = 4.9‰, rhyolite PAN-06-218 with $\delta^{18}O_{pl}$ = 5.9‰, and dacite PAN-06-219 with $\delta^{18}O_{am}$ = 5.2‰.

More O-isotope data are available for the Adakite suite because it was possible to separate amphibole from most samples as well as clinopyroxene and feldspar from some rocks. Based on their young age, we have calculated magmatic $\delta^{18}O$ values for all but two of the 29 Adakite suite samples (see below). The least evolved adakite sample, basaltic andesite PAN-06-141, has a $\delta^{18}O_{cpx}$ value of 5.4‰, which yields a magmatic $\delta^{18}O$ value of 6.1‰ that is consistent with a normal subduction zone mantle origin. Another eight andesites (PAN-06-141; PAN-06-140; PAN-06-175; PAN-06-177; PAN-06-173; PAN-06-006; PAN-06-136; and PAN-06-165) and a dacite (PAN-06-073) have magmatic $\delta^{18}O$ values that fall between 5.7‰ and 6.2‰ indicative of a similar origin. By contrast, the remainder of the Adakite sample suite of 13 andesites and four dacites exhibit surprisingly variable magmatic $^{18}O/^{16}O$ ratios that vary more than 1‰ from $\delta^{18}O$ = 6.4‰ to 7.5‰ and exhibit the same characteristic ^{18}O enrichment observed for adakitic lavas globally (Fig. 11) that were originally described by Abratis and Wörner (2001) and Bindeman et al. (2005). The four Panamanian adakites analyzed by Bindeman et al. (2005) have magmatic $\delta^{18}O$ values of between 6.4‰ and 6.9‰, which fall toward the center of the 5.7‰ to 7.5‰ $\delta^{18}O$ distribution determined here for 27 samples.

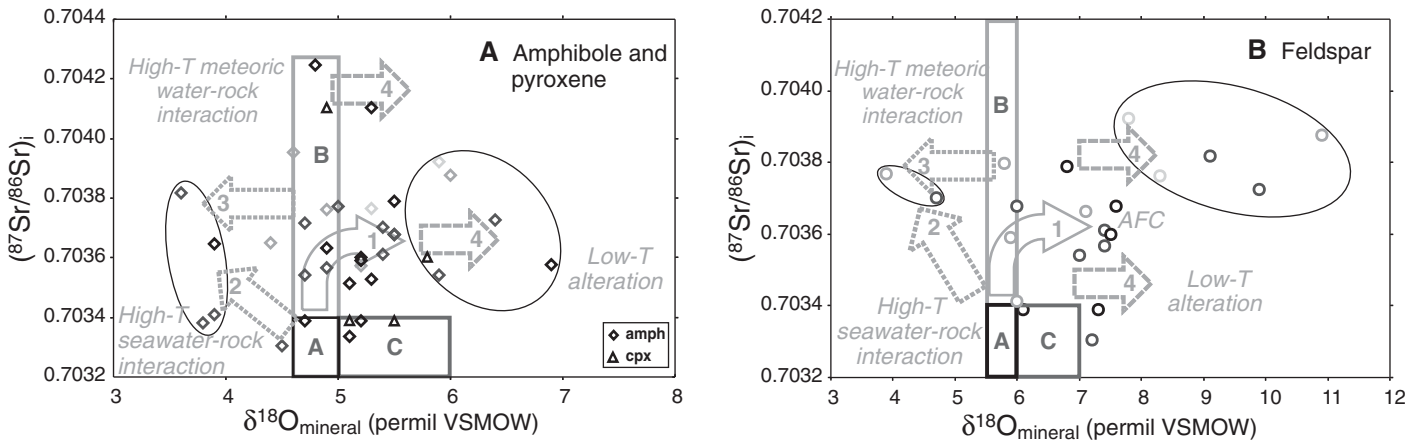

Figure 10. Plot of mineral $^{87}Sr/^{86}Sr$ versus $\delta^{18}O$ for (A) amphibole and pyroxene and (B) feldspar for Panamanian igneous rocks. See text for explanation. The two circles in the figures bound samples that have had their O-isotopic compositions modified by high- and low-temperature secondary processes as indicated in the figure and discussed in the text. VSMOW—Vienna standard mean ocean water. amph—amphibole; cpx—clinopyroxene.

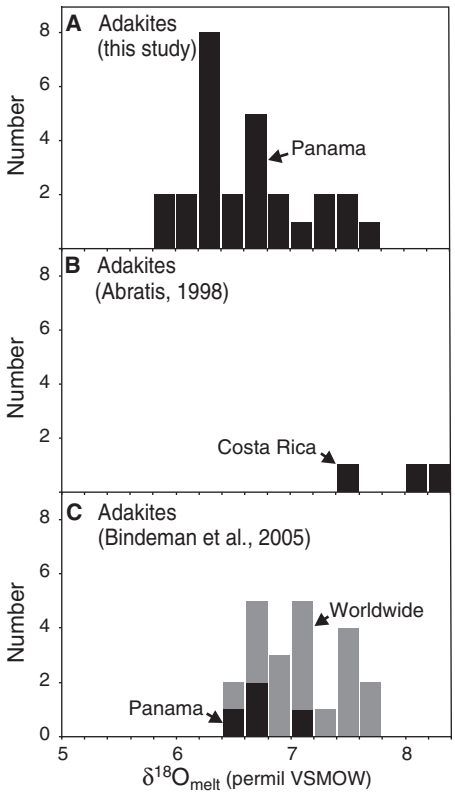

Figure 11. Histogram comparing $\delta^{18}O$ values of Panamanian adakites (A) with those from Costa Rica (B) analyzed by Abratis (1998) and various locations worldwide including Panama (C) analyzed by Bindeman et al. (2005). VSMOW—Vienna standard mean ocean water.

Two samples, PAN-06-043 and PAN-06-044, are compositionally akin to the other dacitic Adakite suite lavas analyzed except that they have unusually high and low $\delta^{18}O_{am}$ values of 6.9‰ and 3.9‰, respectively. These anomalous O-isotopic compositions for phenocrysts in fresh young lavas are difficult to explain but may offer critical insight into the petrogenesis of the Panamanian adakites. Adakites are widely considered to be the result of melting the subducting slab (Kay, 1978; Defant and Drummond, 1990; Stern and Kilian, 1996). Bindeman et al. (2005) have argued that adakites from convergent plate margin settings with modest enrichments in ^{18}O and ^{87}Sr, like those from Panama and Fiji, may be generated through melting of the ^{18}O enriched upper portion of the subducting slab. Since the unusual O-isotope values in Central American adakites are related to strongly elevated Sr-isotope compositions at constant and high Nd-isotope ratios (Abratis, 1998), this signature is considered a clear indication for melting of seawater-altered basaltic rocks within the subducting slab. The broad range of O-isotope ratios observed here for the Panamanian Adakite suite, with $\delta^{18}O_{magma}$ = 5.7‰ to 7.5‰, and the two adakite amphiboles with anomalously high and low $\delta^{18}O_{am}$ values of 6.9‰ and 3.9‰, suggests melting occurred throughout the slab, with both the upper ^{18}O-enriched and lower ^{18}O-depleted zones of the hydrothermally altered basaltic ocean crust involved in the melting process.

Temporal History of Radiogenic Isotope Variations

The radiogenic isotopic data are listed in Tables 4 and 5 and plotted as a function of sample age in Figure 12. Since a careful screening was performed based on the O-isotope data to identify samples affected by post-crystallization alteration, we will now consider in the discussion and interpretation of the radiogenic isotopes that follows only those samples identified to be pristine. A clear temporal trend is observed for Nd-isotope ratios (Fig. 12A), with $^{143}Nd/^{144}Nd$ for the different groups progressively increasing over the past 71 million years. The two Soná-Azuero arc samples have low and uniform Nd-isotope ratios of 0.512864 ± 5 and 0.512866 ± 4. The Chagres-Bayano arc suite displays a larger Nd-isotope variation from 0.512929 ± 4 to 0.512853 ± 4, consistent with large variations in HFSE, distinctly higher compared to the Soná-Azuero arc and Cordilleran arc groups. The Cordilleran arc has Nd-isotope ratios from 0.513000 ± 3 to 0.512963 ± 8 that are significantly higher than those for the Chagres-Bayano arc. The Adakite suite displays a narrow but high range of $^{143}Nd/^{144}Nd$ ratios from 0.513016 ± 9 to 0.512951 ± 4. This progressive increase in $^{143}Nd/^{144}Nd$ ratios over the course of the past 71 million years indicates a more depleted mantle wedge composition through time with respect to Sm/Nd during the evolution of the Central American arc. Similarly, an increase through time toward more radiogenic lead is observed for both $^{206}Pb/^{204}Pb$ and $^{208}Pb/^{204}Pb$ ratios (Figs. 12B and 12C). There is a large difference in Pb-isotope composition between Soná-Azuero arc and Chagres-Bayano arc samples, especially for $^{206}Pb/^{204}Pb$ ratios, whereas the Chagres-Bayano arc and Cordilleran arc samples are of similar Pb-isotopic composition. The Soná-Azuero arc has low $^{206}Pb/^{204}Pb$ ratios of 18.65 ± 0.01 and 18.53 ± 0.008. The Chagres-Bayano arc lavas show distinctly higher values from 19.04 ± 0.002 to 18.78 ± 0.007. The Cordilleran arc is more homogeneous with $^{206}Pb/^{204}Pb$ ratios ranging from 19.03 ± 0.008 to 8.96 ± 0.003. The Adakite suite displays the highest Pb-isotope ratios and largest variation, with $^{206}Pb/^{204}Pb$ ratios ranging from 19.34 ± 0.005 to 18.89 ± 0.003.

The temporal trends for $^{207}Pb/^{204}Pb$ and $^{87}Sr/^{86}Sr$ are not as distinct as those for the other radiogenic isotope systems (Figs. 12D and 12E). On average, $^{207}Pb/^{204}Pb$ ratios are similar in all groups. Variation is again largest for the Adakite suite, mainly due to the high $^{207}Pb/^{204}Pb$ ratios of PAN-06-165 and PAN-06-006. The $^{87}Sr/^{86}Sr$ ratios exhibit an initial decline from Soná-Azuero arc to Chagres-Bayano arc to the oldest Cordilleran arc samples but then trend toward a partial enrichment in ^{87}Sr in the youngest Cordilleran arc rocks. For the Adakite suite, samples PAN-06-165 and PAN-06-073 again contribute to the large Sr-isotopic variation of the Adakite suite samples.

Figure 12 also shows reference fields for the Galápagos spreading center (GSC) from the Petrological Database of the Ocean Floor (PetDB) and the Galápagos southern domain (GSD) from White et al. (1993) as defined by Hoernle et al. (2000). In order to compare magma sources through time, radiogenic isotopic evolution has been calculated back in time. Due to a lack of U, Th, and Pb concentrations for the Galápagos data, we followed the method of Hauff et al. (2000a) and assumed a linear increase of μ with $^{206}Pb/^{204}Pb$ (μ = 10*$^{206}Pb/^{204}Pb$-175) and $^{232}Th/^{238}U$ = 3. In addition, data for rocks of accreted terranes from the hotspot tracks outboard of Central America are also plotted (Sadofsky et al., 2009; Hoernle et al., 2002). Where clear differences exist for $^{206}Pb/^{204}Pb$ and $^{208}Pb/^{204}Pb$ ratios between GSC and GSD, Panama magmas sources are intermediate or displaced from GSC toward GSD indicating that the Galápagos southern domain may have been an important source component throughout the entire magmatic history of central and western Panama from as early as 66 Ma. It is clear from the unsystematic scatter of Sr-isotope ratios, and in particular their higher values relative to both GSD and GSC (Fig. 12), that some Sr-isotope compositions have been affected by seawater, either by introduction to their source or as a consequence of rock alteration after formation.

Radiogenic isotopes are presented in Figure 13 together with reference data for MORB from the southern Eastern Pacific Rise (EPR) and from the Galápagos spreading center (GSC) from literature sources (from the PetDB). Data for the hotspot tracks are taken from Sadofsky et al. (2009) and Hoernle et al. (2002) and for the active Central American arc from Carr et al. (2003), Feigenson et al. (2004), and Hoernle et al. (2008). The global subducted sediment (GLOSS) field is from Plank and Langmuir (1998), and the local sediment field is from Sadofsky et al. (2009) and Feigenson et al. (2004). The Caribbean large igneous province

TABLE 4. INITIAL AND MEASURED Sr- AND Nd-ISOTOPIC COMPOSITION FOR SEPARATED MINERALS

Sample	Phase analyzed	Rb (ppm)	Sr (ppm)	$^{87}Sr/^{86}Sr$ (measured)	±	$^{87}Sr/^{86}Sr$ (initial)	Sm (ppm)	Nd (ppm)	$^{143}Nd/^{144}Nd$ (measured)	±	$^{143}Nd/^{144}Nd$ (initial)
Soná-Azuero arc											
PAN-05-008	Amphibole	2.11	107.64	0.703976	0.000004	0.703923	11.73	38.71	0.512950	0.000005	0.512866
PAN-05-017	Amphibole	0.67	118.97	0.70378	0.000004	0.703764	24.05	65.26	0.512972	0.000004	0.512864
Chagres-Bayano arc											
PAN-03-004	Amphibole	0.34	35.52	0.703329	0.00001	0.703305	13.83	35.62	0.513037	0.000008	0.512939
PAN-03-007	Amphibole	8.28	190.14	0.703787	0.000009	0.703701	10.08	36.05	0.512912	0.000004	0.512855
PAN-03-14-1	Amphibole	0.84	54.45	0.703566	0.00001	0.70354	26.15	78.62	0.512960	0.000004	0.512903
PAN-03-022	Amphibole	1.99	32.02	0.703984	0.000009	0.703819	23.07	59.32	0.512935	0.000004	0.512829
PAN-03-023	Amphibole	0.52	38.87	0.703762	0.000005	0.703726	22.62	64.23	0.512947	0.000005	0.512851
PAN-03-029	Amphibole	1.36	193.02	0.703692	0.000011	0.703679	3.06	5.55	0.513019	0.000004	0.512911
PAN-04-004	Amphibole	2.00	235.78	0.703629	0.000009	0.703612	3.50	7.27	0.513023	0.000009	0.512925
PAN-04-011	Amphibole	18.02	79.95	0.703994	0.00001	0.703567	11.65	33.15	0.512921	0.000004	0.512853
PAN-06-100	Amphibole	0.61	86.44	0.7034	0.000006	0.703382	47.45	109.31	0.513019	0.000005	0.512902
PAN-06-103	Amphibole	0.80	163.43	0.703551	0.000003	0.703542	35.56	51.04	0.512975	0.000004	0.512846
PAN-06-104	Amphibole	0.89	132.08	0.703424	0.000005	0.70341	39.95	98.66	0.513008	0.000002	0.512925
PAN-06-206	Amphibole	0.58	48.29	0.703739	0.000005	0.703715	57.70	162.07	0.512975	0.000005	0.512902
PAN-06-210	Amphibole	0.48	56.85	0.703789	0.000006	0.703773	23.02	51.39	0.513016	0.000004	0.512929
Cordilleran arc											
PAN-03-032	Amphibole	3.89	91.91	0.703901	0.000011	0.703876	15.99	45.27	0.512923	0.000004	0.512902
PAN-05-031	Feldspar	8.51	1648.81	0.703801	0.000003	0.703799	1.47	7.29	0.512983	0.000005	0.512973
PAN-05-056	Feldspar	0.48	1568.52	0.703413	0.000005	0.703413	0.47	3.07	0.513012	0.000003	0.513
PAN-06-023	Amphibole	8.92	2562.84	0.703953	0.000006	0.703952	27.01	102.98	0.512967	0.000004	0.512959
PAN-06-041	Matrix	84.92	751.68	0.704094	0.000003	0.70403	11.92	47.72	0.512986	0.000005	0.512971
PAN-06-068	Amphibole	1.77	120.71	0.703653	0.000004	0.703649	30.13	114.61	0.513007	0.000008	0.513
PAN-06-125	Feldspar	3.72	2148.59	0.703665	0.000002	0.703665	0.27	3.69	0.512962	0.000008	0.51296
PAN-06-131	Amphibole	2.02	322.26	0.703763	0.000003	0.703761	62.91	233.66	0.512973	0.000008	0.512963
PAN-06-185a	Feldspar	29.89	2089.85	0.703774	0.000008	0.703769	1.24	9.24	0.512960	0.00001	0.512955
PAN-06-218	Feldspar	1.25	1446.83	0.703591	0.000005	0.703591	0.46	5.80	0.512989	0.000005	0.512985
PAN-06-219	Amphibole	2.52	156.90	0.70358	0.000004	0.703572	36.92	107.07	0.513016	0.000004	0.512999
Adakite suite											
PAN-05-047	Amphibole	5.14	2010.86	0.703677	0.000004	0.703677	33.31	145.72	0.512963	0.000002	0.512963
PAN-05-049	Amphibole	2.82	247.86	0.703769	0.00001	0.70379	98.16	351.08	0.512973	0.000004	0.512973
PAN-06-006	Amphibole	5.01	549.94	0.703516	0.00001	0.703516	82.96	127.58	0.512967	0.000002	0.512963
PAN-06-010	Amphibole	1.08	62.78	0.703529	0.000004	0.703528	41.26	96.10	0.512982	0.000002	0.512979
PAN-06-014	Amphibole	8.32	2241.16	0.703633	0.000002	0.703633	24.05	112.40	0.512961	0.000005	0.51296
PAN-06-043	Amphibole	16.86	607.82	0.703578	0.000006	0.703577	44.05	45.83	0.513004	0.000007	0.513001
PAN-06-044	Amphibole	26.81	327.46	0.703648	0.000004	0.703645	13.66	51.74	0.512984	0.000008	0.512983
PAN-06-073	Amphibole	1.81	693.15	0.704246	0.00001	0.704248	19.06	68.26	0.513009	0.00001	0.513007
PAN-06-136	Amphibole	3.36	5930.28	0.703336	0.000009	0.703336	17.39	60.02	0.512955	0.000004	0.512955
PAN-06-165	Amphibole	4.90	1820.75	0.704103	0.000003	0.704103	29.08	115.73	0.512982	0.000007	0.512981
PAN-06-166	Amphibole	4.35	1134.61	0.703389	0.000003	0.703389	9.92	32.55	0.512964	0.000003	0.512964
PAN-06-168	Amphibole	2.06	912.10	0.70359	0.000005	0.70359	7.95	28.41	0.513016	0.000009	0.513016
PAN-06-176	Amphibole	3.56	940.78	0.7036	0.000003	0.7036	9.15	31.94	0.512963	0.000004	0.512962
PAN-06-177	Amphibole	3.32	5106.91	0.703389	0.000003	0.703389	13.01	45.72	0.512952	0.000004	0.512951

data are from Kerr et al. (1997, 2002) and Hauff et al. (2000a, 2000b).

Initial isotope ratios were calculated based on parent/daughter ratios of Rb/Sr, Sm/Nd, and U/Pb and Th/Pb measured by ICP-MS for single crystal aliquots from each sample. The mean error for Rb/Sr is 7% and for Sm/Nd 6%. U and Th for most samples were below the detection limit of 0.01 ppm for U and 0.03 ppm for Th for ICP-MS. Therefore we used these values as an upper boundary for U and Th and Pb as measured for our initial calculation. The differences between measured and initial values are negligible for most samples, except for eight samples that have particularly low values of Pb.

The $^{143}Nd/^{144}Nd$-$^{87}Sr/^{86}Sr$ plot (Fig. 13A) and the $^{143}Nd/^{144}Nd$-$^{206}Pb/^{204}Pb$ plot (Fig. 13B) both show clearly that the Chagres-Bayano arc has a radiogenic isotopic character that is similar to the Caribbean large igneous province. The two Chagres-Bayano arc samples PAN-03-007 and PAN-04-011 with low $^{143}Nd/^{144}Nd$ have pristine $\delta^{18}O_{melt}$ values only slightly above the mantle reference value (5.6‰ ± 0.2‰). This indicates that the low $^{143}Nd/^{144}Nd$ signature observed for the Chagres-Bayano arc rocks is a source signal and not a result of assimilation in the arc crust. The displacement of the Panama field toward GLOSS and the local sediments in Figure 13 is likely caused by subducted sediment melts in the Chagres-Bayano arc source, a feature that is consistent with the variable HFSE contents and Th/La ratios of Chagres-Bayano arc magmas. These sediments, however, would have to have been relatively nonradiogenic with respect to Pb isotopes (Figs. 13D and 13E). The Soná-Azuero arc is very similar isotopically in the $^{143}Nd/^{144}Nd$-$^{87}Sr/^{86}Sr$ plot (Fig. 13A), but it is clearly less radiogenic than the Chagres-Bayano arc in terms of its Pb-isotope composition (Figs. 13D and 13E). Caribbean large igneous province rocks are enriched in ^{87}Sr, probably as a consequence of seawater interaction or possibly a contribution from subducted sediments (low $^{143}Nd/^{144}Nd$ subfield in Fig. 13A). Most probably, Caribbean large igneous province and Chagres-Bayano arc magmas were derived from a source that contained a mixture of depleted MORB mantle (DMM) and an enriched, slab component such as subducted sediments and/or melts thereof. In terms of their Nd- and Sr-isotope compositions (Fig. 13A), the Cordilleran arc samples plot into the Central American arc and Caribbean large igneous province fields. The higher $^{143}Nd/^{144}Nd$ values for the Cordilleran arc and Adakite suite compared to the Soná-Azuero arc and Chagres-Bayano arc probably reflect a more primitive mantle source in a less mature arc system that had been affected by a lower degree of slab component enrichment.

In $^{143}Nd/^{144}Nd$ versus $^{206}Pb/^{204}Pb$ space (Fig. 13B), the Cordilleran arc plots largely coincident with the Central American arc and accreted OIB fields, whereas the Adakite suite closely follows the trend of the hotspot track samples

TABLE 5. INITIAL AND MEASURED Pb-ISOTOPIC COMPOSITION FOR SEPARATE MINERALS

Sample	Material	U (ppm)	Th (ppm)	Pb (ppm)	$^{206}Pb/^{204}Pb$ (measured)	±	$^{206}Pb/^{204}Pb$ (initial)	$^{207}Pb/^{204}Pb$ (measured)	±	$^{207}Pb/^{204}Pb$ (initial)	$^{208}Pb/^{204}Pb$ (measured)	±	$^{208}Pb/^{204}Pb$ (initial)
Soná-Azuero arc													
PAN-05-008	Amphibole	<0.01	<0.03	0.49	18.659	0.012	18.65	15.615	0.010	15.614	38.418	0.026	38.405
PAN-05-017	Amphibole	<0.01	<0.03	<0.03	18.766	0.010	18.528	15.657	0.008	15.57	38.553	0.020	38.113
Chagres-Bayano arc													
PAN-03-004	Amphibole	<0.01	<0.03	0.17	19.004	N.D.	18.981	15.681	N.D.	15.68	38.700	N.D.	38.665
PAN-03-007	Amphibole	<0.01	<0.03	0.75	18.976	0.047	18.972	15.568	0.039	15.568	38.683	0.096	38.677
PAN-03-14-1	Amphibole	<0.01	<0.03	0.41	18.882	0.002	18.876	15.565	0.002	15.565	38.445	0.005	38.435
PAN-03-022	Amphibole	<0.01	<0.03	0.89	18.820	0.010	18.815	15.573	0.008	15.573	38.428	0.020	38.42
PAN-03-023	Amphibole	<0.01	<0.03	0.33	19.078	0.006	19.065	15.595	0.005	15.595	38.848	0.012	38.828
PAN-03-029	Amphibole	<0.01	<0.03	0.26	18.928	0.047	18.916	15.575	0.039	15.574	38.619	0.096	38.601
PAN-04-004	Amphibole	<0.01	<0.03	0.30	18.933	0.025	18.923	15.539	0.021	15.539	38.529	0.052	38.513
PAN-04-011	Amphibole	<0.01	<0.03	2.51	19.040	0.007	19.039	15.566	0.006	15.566	38.745	0.015	38.743
PAN-06-100	Amphibole	<0.01	<0.03	<0.03	18.692	0.007	18.748	15.645	0.006	15.584	38.490	0.015	38.327
PAN-06-103	Amphibole	<0.01	<0.03	0.64	19.025	0.020	19.02	15.697	0.016	15.697	38.854	0.040	38.847
PAN-06-104	Amphibole	<0.01	<0.03	0.62	18.984	0.003	18.979	15.596	0.002	15.596	38.593	0.006	38.585
PAN-06-206	Amphibole	<0.01	<0.03	<0.03	18.935	0.007	18.778	15.657	0.006	15.59	38.841	0.015	38.499
PAN-06-210	Amphibole	<0.01	<0.03	<0.03	18.643	0.007	18.811	15.671	0.006	15.608	38.635	0.014	38.579
Cordilleran arc													
PAN-03-032	Amphibole	<0.01	<0.03	0.42	19.120	0.001	19.118	15.569	0.001	15.569	38.806	0.003	38.803
PAN-05-031	Feldspar	<0.01	<0.03	2.30	18.956	0.003	18.956	15.593	0.002	15.593	38.728	0.005	38.728
PAN-05-056	Feldspar	<0.01	<0.03	1.20	19.034	0.008	19.033	15.644	0.007	15.644	38.828	0.017	38.826
PAN-06-023	Amphibole	0.09	0.35	1.47	18.986	0.005	18.981	15.622	0.004	15.622	38.810	0.011	38.804
PAN-06-041	Matrix	1.97	5.58	9.69	18.818	0.003	18.787	15.594	0.003	15.593	38.581	0.007	38.552
PAN-06-068	Amphibole	0.08	0.22	0.71	19.046	0.008	19.037	15.607	0.006	15.607	38.766	0.016	38.758
PAN-06-125	Feldspar	<0.01	<0.03	16.03	19.012	0.002	19.012	15.572	0.002	15.572	38.696	0.005	38.696
PAN-06-131	Amphibole	<0.01	<0.03	0.96	18.995	0.004	18.994	15.594	0.003	15.594	38.721	0.008	38.72
PAN-06-185a	Feldspar	<0.01	<0.03	9.25	19.075	0.005	19.075	15.647	0.004	15.647	38.924	0.010	38.924
PAN-06-218	Feldspar	<0.01	<0.03	5.43	18.960	0.008	18.96	15.624	0.006	15.623	38.770	0.016	38.77
PAN-06-219	Amphibole	<0.01	<0.03	<0.03	19.048	0.009	19.02	15.607	0.007	15.605	38.740	0.018	38.697
Adakite suite													
PAN-05-047	Amphibole	<0.01	<0.03	1.50	19.126	0.009	19.126	15.661	0.008	15.661	38.964	0.019	38.964
PAN-05-049	Amphibole	<0.01	<0.03	1.56	19.081	0.006	19.081	15.612	0.005	15.612	38.820	0.012	38.82
PAN-06-006	Amphibole	<0.01	<0.03	3.23	19.270	0.008	19.27	15.685	0.007	15.685	39.133	0.017	39.133
PAN-06-010	Amphibole	<0.01	<0.03	0.72	19.140	0.009	19.139	15.568	0.007	15.568	38.824	0.018	38.823
PAN-06-014	Amphibole	0.35	0.85	3.08	19.139	0.003	19.138	15.613	0.002	15.613	38.912	0.005	38.912
PAN-06-043	Amphibole	<0.01	<0.03	8.32	19.151	0.004	19.151	15.624	0.004	15.624	38.897	0.009	38.897
PAN-06-044	Amphibole	0.53	1.80	4.29	18.956	0.006	18.955	15.620	0.005	15.62	38.739	0.012	38.737
PAN-06-073	Amphibole	0.17	0.23	0.73	18.917	0.027	19.049	15.813	0.023	15.584	38.992	0.056	38.738
PAN-06-136	Amphibole	<0.01	<0.03	1.85	19.324	0.006	19.324	15.598	0.005	15.598	39.066	0.012	39.066
PAN-06-165	Amphibole	<0.01	<0.03	1.51	19.289	0.013	19.289	15.716	0.010	15.716	39.235	0.026	39.235
PAN-06-166	Amphibole	<0.01	<0.03	0.98	18.892	0.003	18.892	15.604	0.002	15.604	38.687	0.006	38.687
PAN-06-168	Amphibole	<0.01	<0.03	<0.03	19.138	0.002	19.138	15.575	0.001	15.575	38.804	0.003	38.804
PAN-06-176	Amphibole	<0.01	<0.03	<0.03	19.214	0.005	19.212	15.625	0.004	15.625	38.990	0.011	38.988
PAN-06-177	Amphibole	<0.01	<0.03	<0.03	19.345	0.007	19.342	15.608	0.006	15.608	39.080	0.014	39.076

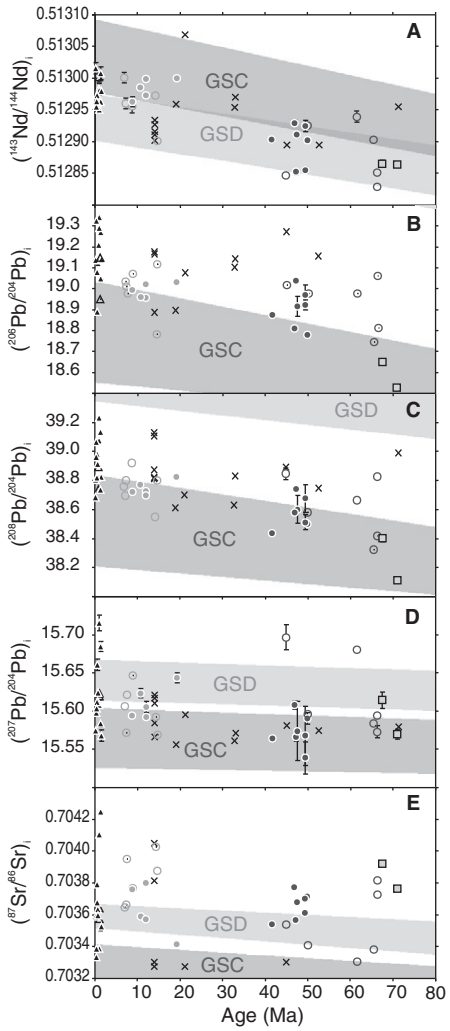

Figure 12. (A–E) Plot of Pb-, Nd-, and Sr-isotope ratios for igneous rocks from central and western Panama over the past 80 million years. Open symbols are altered samples based on mineral $\delta^{18}O$ values. The light-gray field shows reference data for the GSC—Galápagos spreading center (compilation from the PetDB [Petrological Database of the Ocean Floor]: http://www.petdb.org/petdbWeb/search/download_pg.jsp), and the dark-gray field shows reference data for the southern Galápagos domain defined by Hoernle et al. (2000) together with data from White et al. (1993). Isotopic evolution has been calculated back in time. Due to a lack of U, Th, and Pb concentrations for the Galápagos data, we followed the method of Hauff et al. (2000a) assuming a linear increase with $^{206}Pb/^{204}Pb$ ($\mu = 10*^{206}Pb/^{204}Pb\text{-}175$) and $^{232}Th/^{238}U = 3$ to allow for comparison of magma sources. Crosses represent data for rocks from accreted hotspot track from Sadofsky et al. (2009) and Hoernle et al. (2002).

and their plume mantle source. The Adakite suite consists of the Panama samples that have the most radiogenic Pb-isotopic composition (Figs. 13D and 13E) and thus most directly reflect the melting of Caribbean large igneous province basement or subducted Galápagos seamount basalts, both of which would carry the Galápagos plume source signature (Abratis and Wörner, 2001; Bindeman et al., 2005). Lavas of the Adakite suite also are enriched in ^{18}O, with $\delta^{18}O$ values up to 7‰, a feature that suggests a magma source component that was strongly affected by low-temperature seawater alteration. Significant crustal input (i.e., sediment subduction or assimilation) is not consistent with the relatively high and uniform Adakite suite $^{143}Nd/^{144}Nd$ ratios.

Overall, our sample suite can be described in terms of four geochemical components, each of which contributed to arc magmatism in Panama during the past 71 Ma. It is noteworthy that Soná-Azuero arc rocks, which represent the onset of subduction at the western margin of the Caribbean large igneous province plateau, show the highest sediment component, whereas the young Adakite suite magmatism has the strongest signature from a (seawater-modified) Galápagos source with only minor sediment addition. The Chagres-Bayano arc and Cordilleran arc samples fall between these two end-member situations and mix toward a depleted mantle. Three mantle components have contributed to Panamanian magmatism: (1) depleted asthenospheric mantle that is present in all groups, (2) subducted sediments that produced an enriched isotopic signature in the Soná-Azuero arc and Chagres-Bayano arc, and (3) a Galápagos-plume type source, which is strongly manifest in the Adakite suite and of only minor significance for the Chagres-Bayano arc and Cordilleran arc magma sources. An additional ^{87}Sr-enriched component (4) is recognized that reflects a seawater contribution to Adakite suite magmagenesis and hydrothermal alteration of the other age groups after their emplacement. A ubiquitous, slab-derived, LILE-enriched and HFSE-depleted fluid is present in all rocks.

Changing Mantle Sources through Time

Initial Caribbean large igneous province magmatism was derived from a plume mantle source and resulted in the thickening of the Caribbean oceanic crust over a period of ~25 million years from ~95 to 71 Ma (Hoernle et al., 2004). The second, Chagres-Bayano arc phase of magmatism from 66 to 42 Ma was generated within a subduction-modified depleted mantle source. Significant amounts of oceanic sediment were subducted and mixed into this depleted mantle during the initiation of the Panama arc. The earliest Soná-Azuero arc (71–68 Ma) samples are still geochemically distinct in this scenario. They display trace element characteristics that more closely resemble the OIB-like Caribbean large igneous province basement than the rocks of Chagres-Bayano arc (Figs. 7 and 8) because they are less depleted in radiogenic isotope character than Chagres-Bayano arc samples. Because the Soná-Azuero arc represents the transition from plume activity at the Galápagos hotspot to subduction, the mantle wedge at that time may still have contained a component of enriched Caribbean large igneous province mantle, but also had a significant contribution from subducted sediments. This idea is supported by Buchs et al. (2007), who found arc rocks on the Azuero peninsula with REE compositions similar to the composition of the Caribbean large igneous province plateau. They concluded that these proto-arc magmas were derived from the subplateau lithospheric mantle. During Chagres-Bayano arc time (66–42 Ma), the mantle source producing arc magmas was still immature and compositionally variable, possibly reflecting the progressive establishment and progressive maturation of the arc system by variable compositions of mantle wedge and sediment components. After a significant temporal gap in arc magmatic activity, the Cordilleran arc lavas erupted from 19 to 7 Ma (our new Ar-Ar ages) and reflect a less depleted mantle source compared to that which produced the Chagres-Bayano arc magmas. The final Adakite suite phase of magmatism during the past 2 million years is distinct because magma generation is largely independent of mantle wedge composition. Adakite suite magmas likely formed by melting the leading edge of the subducted Cocos Ridge and older Caribbean large igneous province basement, either at the margin of a slab window or after slab breakoff below west-central Panama (Johnston and Thorkelson, 1997; Abratis and Wörner, 2001).

Initiation of arc magmatism ~70 Ma, at the same time as formation of the Galápagos plateau ended, removes the structural problem of forming Galápagos-plateau rocks on the Caribbean side of the proto–Central American arc. It was this issue that led Pindell et al. (2006) to argue against a link between the Galápagos hotspot and the thickened Caribbean plate. This temporal coincidence may, in fact, suggest a causal link.

The change in magma source character from Chagres-Bayano arc to Cordilleran arc magmatism, defined by trace element composition, is mostly a trajectory toward a more evolved parental magma composition. This could indicate

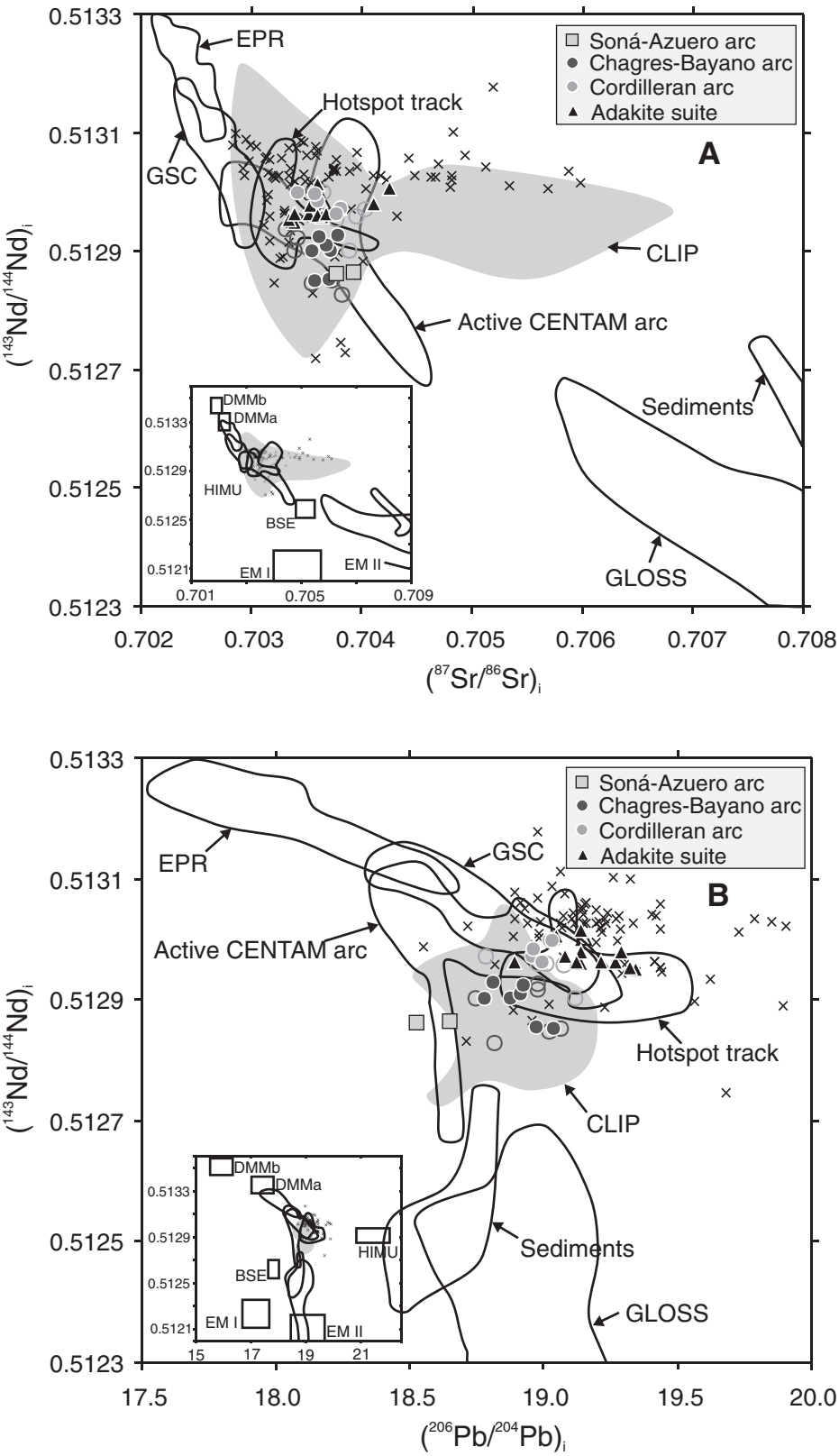

Figure 13 (*on this and following two pages*). Plots of initial Sr-, Nd-, and Pb-isotope ratios for magmatic rocks of western and central Panama (A–E) together with reference fields for initial and measured Caribbean large igneous province (CLIP) (data from Kerr et al., 1997, 2002; Hauff et al., 2000a). GLOSS—Global Subducted Sediment (Plank and Langmuir, 1998); sediment—local sediments (Sadofsky et al., 2009; Feigenson et al., 2004); active CENTAM arc—active Central American arc (Carr et al., 2003; Feigenson et al., 2004; Hoernle et al., 2008); EPR—East Pacific Rise; and GSC—Galápagos spreading center (both from the PetDB [Petrological Database of the Ocean Floor]: http://www.petdb.org/petdbWeb/search/download_pg.jsp), and the initial hotspot track data (Sadofsky et al., 2009; Hoernle et al., 2002). The reference field for Caribbean large igneous province is subdivided into two parts: gray shaded—initial values and gray crosses—measured values. The inset on each figure shows the data relative to the mantle reference fields (Zindler and Hart, 1986) for depleted mantle—DMMa and DMMb; enriched mantle—EMI and EMII; bulk silicate earth—BSE; and the enriched Pb reservoir—HIMU. Open symbols are altered samples based on mineral $\delta^{18}O$ values. Analytical uncertainly is smaller than the size of data symbols.

increased mixing and homogenization of subarc magma sources with time and/or the replacement of the mantle wedge by homogeneous, relatively undepleted asthenospheric mantle. The breakup of the Farallon plate at ~25 Ma (Lonsdale, 2005) which preceded the onset of the Cordilleran arc (22–19 Ma) may have been the trigger for these changes. The newly established Cocos-Nasca spreading center led to a change in mantle dynamics, for example upwelling in the region below the new ridge. The direction of plate movement also changed between 22.7 and 19.5 Ma, from mainly westward for the Farallon plate to northwest for the Cocos plate and southwest for the Nazca plate (Barckhausen et al., 2008). This rearrangement in relative plate motions caused the changes in mantle source after the breakup. We note that these changes are partly coincident to gaps in the magmatic activity and probably occurred relatively rapidly. This suggests that mantle source changes may have been triggered forcibly by the rearrangement of the plate tectonic setting and

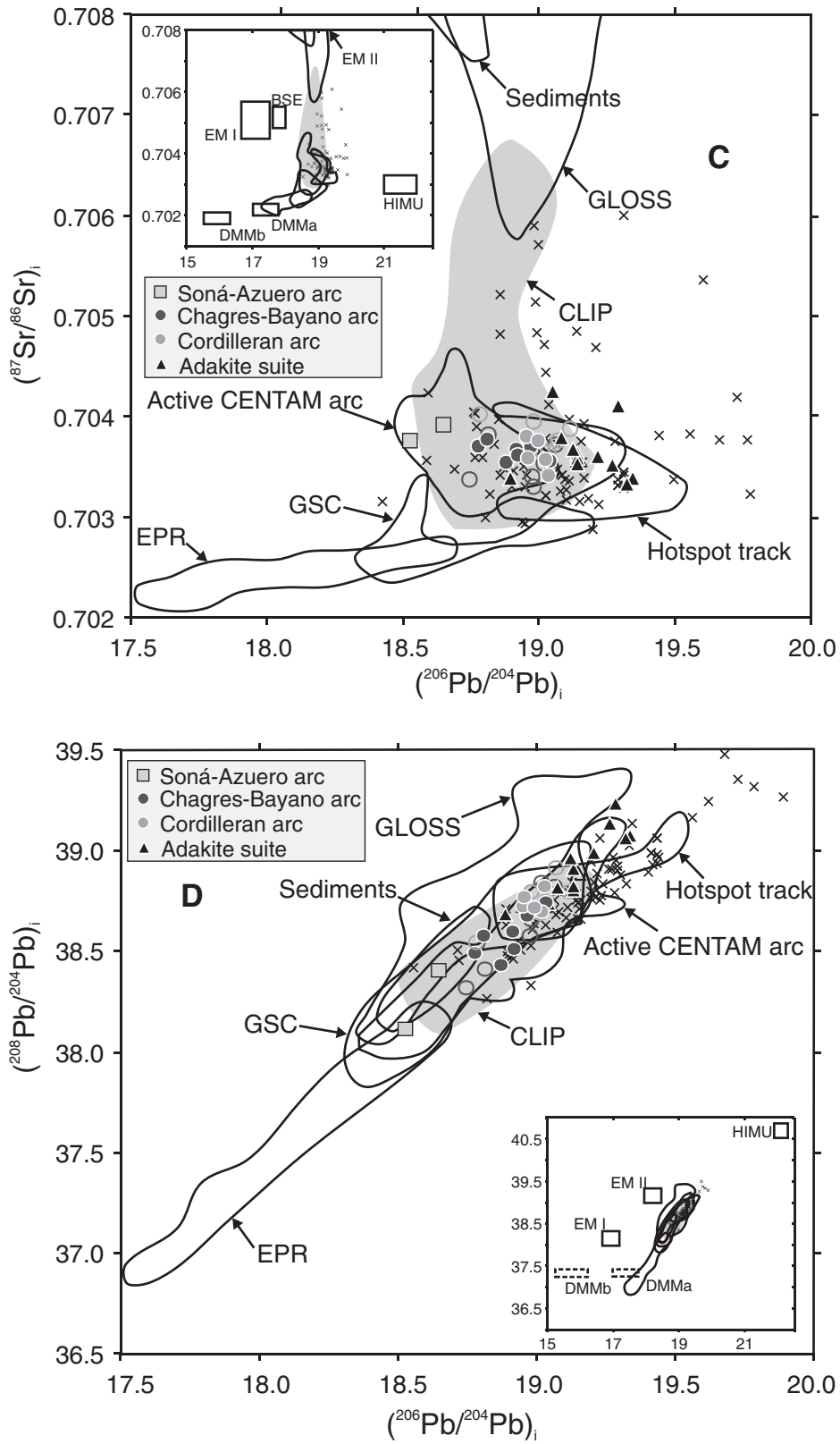

Figure 13 (*continued*).

that the mantle wedge must have been relatively mobile in responding to these dynamic changes of plate configurations.

CONCLUSIONS

A mantle source composed of the old Caribbean large igneous province source and variable degrees of a mixed-plume source is inferred for the Soná-Azuero arc, which represents the switch from island arc volcanism to subduction zone magmatism, with arc magmatism in the region of the Azuero and Soná peninsulas of Panama commencing as early as 71 Ma. The developing arc then migrated eastward into the Chagres-Bayano region of central Panama east of the Panama Canal. During this time, magmas were derived from a variably depleted, subarc mantle source. Subsequently, as the arc system matured, the subarc mantle source evolved toward a slightly more homogeneous and less depleted state. The two phases of Chagres-Bayano arc of magmatism, from 66.4 to 61.5 Ma and from 49.4 to 41.6 Ma, are both distinct in terms of $^{206}Pb/^{204}Pb$ isotope ratios from the earlier Soná-Azuero arc magmatism. This heterogeneous mantle source for Chagres-Bayano arc magmatism consisted of a mixture of depleted mantle and enriched crustal components, most likely derived from variable amounts of subducted marine pelagic sediments and subduction fluids. After a temporal lull of some 20 million years, the Cordilleran arc stage of magmatism commenced at 19.2 Ma and lasted until 6.8 Ma (our new Ar-Ar ages). The mantle source at this time was similar in composition to that which is presently generating magmas below the active Central American arc to the west in Costa Rica. This mantle source for this magmatism was less depleted in composition and tended to produce magmas of a more homogeneous intermediate composition. The difference between Chagres-Bayano arc and Cordilleran arc source compositions reflects a maturation of the subarc mantle as indicated by increased mixing and homogenization of subarc magma sources through time and/or the replacement of the mantle wedge by a homogeneous and relatively undepleted asthenospheric mantle source. For the most recent Adakite suite magmatism in western and central Panama (<2 Ma), an origin is envisioned from partial melts of seawater altered subducted basaltic oceanic crust derived from the Galápagos hotspot mantle.

Changes in subduction style and resultant variations in magma sources are attributed to dynamic changes in regional tectonics over the past 100 million years. The initiation of Soná-Azuero arc magmatism partly overlaps in time

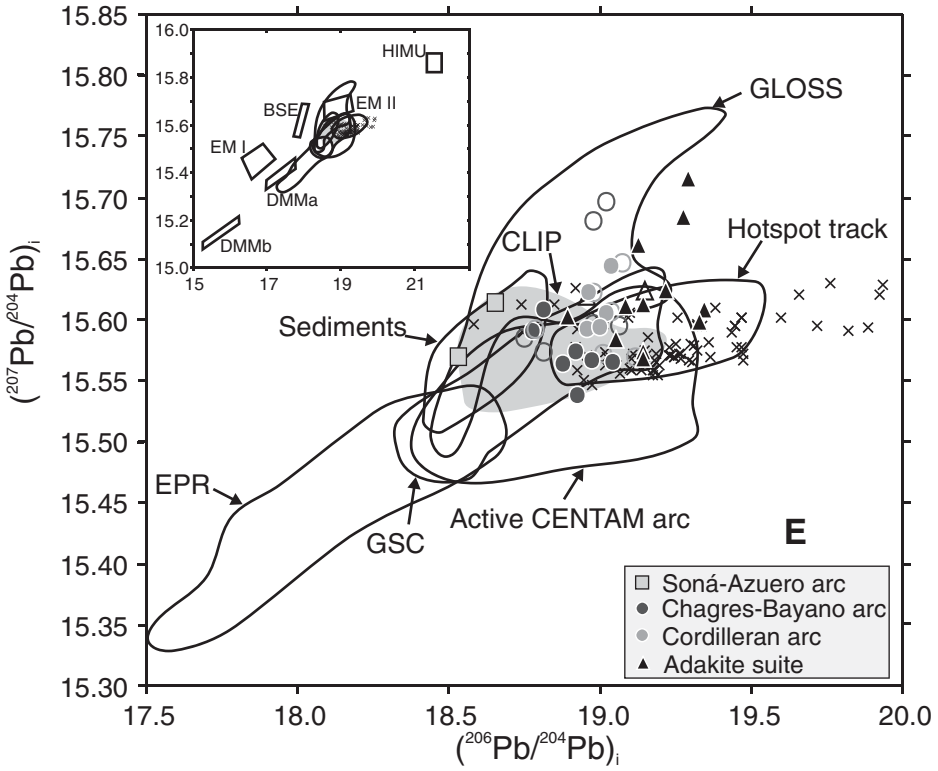

Figure 13 (*continued*).

the cessation of the high plume activity at the Galápagos hotspot. The change from Chagres-Bayano arc to Cordilleran arc magmatism was likely triggered by the breakup of the Farallon plate at ~25 Ma. Changes in contributing mantle sources appear to be relatively abrupt, indicating that the mantle source in the subduction wedge may have been moved forcibly by these plate rearrangements. Adakite suite magmatism was only possible because of slab window formation and accompanied melting of Caribbean large igneous province basement components or Cocos Ridge OIB by intensive slab hydration.

ACKNOWLEDGMENTS

We thank the following organizations and people for their logistical assistance and help in collection of samples across Panama from 2001 to 2006: Thomas Exenberger and Thomas Jakits of Helipan Panama; Lance Vander Zyl of U.S. Army Yuma Proving Ground Tropic Regions Test Center; Eric Nicolaisen, Ricardo Martinez, and Alonso Iglesias of TRAX Evaluación Ambiental, S.A. The Volcan Barú samples were collected and partially analyzed by S. Rausch as a part of her Master's thesis at Göttingen University. G. Hartmann, R. Przybilla, I. Reuber, I. Schönberg, and K. Simon assisted with geochemical and isotopic analytical work. We thank B. Hansen and A. Pack for access to the thermal ionization mass spectrometer and stable isotope laboratories. Financial support for the fieldwork came from an Army Research Laboratory fellow stipend to R.S.H. and from the Deutsche Forschungsgemeinschaft project WO 362/27-2 to G.W. Constructive comments by K. Hoernle and E. Gazel are greatly appreciated.

REFERENCES CITED

Abratis, M., 1998, Geochemical variations in magmatic rocks from southern Costa Rica as a consequence of Cocos Ridge subduction and uplift of the Cordillera de Talamanca [Ph.D. thesis]: University of Göttingen, 144 p.

Abratis, M., and Wörner, G., 2001, Ridge collision, slab-window formation, and the flux of Pacific asthenosphere into the Caribbean realm: Geology, v. 29, p. 127–130, doi: 10.1130/0091-7613(2001)029<0127:RCSWFA>2.0.CO;2.

Alvarado, G.E., Kussmaul, S., Chiesa, S., Gillot, P.Y., Appel, H., Wörner, G., and Rundle, C., 1992, Resumen cronoestratigráfico de las rocas ígneas de Costa Rica basado en dataciones radiométricas: Journal of South American Earth Sciences, v. 6, p. 151–168, doi: 10.1016/0895-9811(92)90005-J.

Alvarado, G.E., Denyer, P., and Sinton, C.W., 1997, The 89 Ma Tortugal komatiitic suite, Costa Rica: Implications for a common geological origin of the Caribbean and Eastern Pacific region from a mantle plume: Geology, v. 25, p. 439–442, doi: 10.1130/0091-7613(1997)025<0439:TMTKSC>2.3.CO;2.

Barckhausen, U., Ranero, C.R., Cande, S.C., Engels, M., and Weinrebe, W., 2008, Birth of an intraoceanic spreading center: Geology, v. 36, p. 767–770.

Bindeman, I.N., Ponomareva, V.V., Bailey, J.C., and Valley, J.W., 2004, Volcanic arc of Kamchatka: A province with high-$\delta^{18}O$ magma sources and large-scale $^{18}O/^{16}O$ depletion of the upper crust: Geochimica et Cosmochimica Acta, v. 68, p. 841–865, doi: 10.1016/j.gca.2003.07.009.

Bindeman, I.N., Eiler, J.M., Yogodzinski, G.M., Tatsumi, Y., Stern, C.R., Grove, T.L., Portnyagin, M., Hoernle, K., and Danyushevsky, L.V., 2005, Oxygen isotope evidence for slab melting in modem and ancient subduction zones: Earth and Planetary Science Letters, v. 235, no. 3–4, p. 480–496, doi: 10.1016/j.epsl.2005.04.014.

Buchs, D.M., Baumgartner, P.O., and Arculus, R., 2007, Late Cretaceous arc initiation on the edge of an oceanic plateau (south Central America): American Geophysical Union, Fall Meeting 2007, abstract T13C-1468.

Carr, M., Feigenson, M., Patino, L., and Walker, J., 2003, Volcanism and geochemistry in Central America: Progress and problems, *in* Eiler, J.M., ed., Inside the Subduction Factory: American Geophysical Union, Geophysical Monograph Series, v. 133, p. 153–174.

Cerling, T.E., Brown, F.H., and Bowman, J.R., 1985, Low-temperature alteration of volcanic glass: Hydration, Na, K, ^{18}O and Ar mobility: Chemical Geology, v. 52, p. 281–293.

Chacko, T., Cole, D.R., and Horita, J., 2001, Equilibrium oxygen, hydrogen, and carbon isotope fractionation factors applicable to geologic systems: Reviews in Mineralogy and Geochemistry, v. 43, p. 1–81, doi: 10.2138/gsrmg.43.1.1.

Chiba, H., Chacko, T., Clayton, R.N., and Goldsmith, J.R., 1989, Oxygen isotope fractionations involving diopside, forsterite, magnetite and calcite: Application of geothermometry: Geochimica et Cosmochimica Acta, v. 53, p. 2985–2995, doi: 10.1016/0016-7037(89)90174-9.

Christie, D.M., Duncan, R.A., McBirney, A.R., Richards, M.A., White, W.M., Harpp, K.S., and Fox, C.G., 1992, Drowned islands downstream from the Galápagos hotspot imply extended speciation times: Nature, v. 355, p. 246–248, doi: 10.1038/355246a0.

Coates, A.G., Jackson, J.B.C., Collins, L.S., Cronin, T.M., Dowsett, H.J., Bybell, L.M., Jung, P., and Obando, J.A., 1992, Closure of the Isthmus of Panama: The near-shore marine record of Costa Rica and western Panama: Geological Society of America Bulletin, v. 104, p. 814–828, doi: 10.1130/0016-7606(1992)104<0814:COTIOP>2.3.CO;2.

Coates, A.G., Aubry, M., Berggren, W., and Collins, L., 2000, New evidence for the earliest stages in the rise of the Isthmus of Panama from Bocas del Toro, Panama: Geological Society of America, 2000 Annual Meeting Abstracts with Program, v. 32, p. A-146.

Collins, L.S., Coates, A.G., Berggren, W.A., Aubry, M.-P., and Zhang, J., 1996, The late Miocene Panama isthmian strait: Geology, v. 24, p. 687–690, doi: 10.1130/0091-7613(1996)024<0687:TLMPIS>2.3.CO;2.

de Boer, J.Z., Defant, M.J., Stewart, R.H., Restrepo, J.F., Clark, L.F., and Ramirez, A.H., 1988, Quaternary calc-alkaline volcanism in western Panama: Regional variation and implication for the plate tectonic framework: Journal of South American Earth Sciences, v. 1, p. 275–293, doi: 10.1016/0895-9811(88)90006-5.

de Boer, J.Z., Defant, M.J., Stewart, R.H., and Bellon, H., 1991, Evidence for active subduction below western Panama: Geology, v. 19, p. 649–652, doi: 10.1130/0091-7613(1991)019<0649:EFASBW>2.3.CO;2.

de Boer, J.Z., Drummond, M., Bordelon, M.J., Defant, M.J., Bellon, H., and Maury, R.C., 1995, Cenozoic magmatic phases of the Costa Rican island arc (Cordillera de Talamanca), *in* Mann, P., ed., Geologic and Tectonic Development of the Caribbean Plate Boundary in Southern Central America: Geological Society of America Special Paper 262, p. 35–55.

Defant, M.J., and Drummond, M.S., 1990, Derivation of some modern arc magmas by melting of young subducted lithosphere: Nature, v. 347, p. 662–665, doi: 10.1038/347662a0.

Defant, M.J., Clark, L.F., Stewart, R.H., Drummond, M.S., de Boer, J.Z., Maury, R.C., Bellon, H., Jackson, T., and Restrepo, J.F., 1991a, Andesite and dacite genesis via contrasting processes: The geology and geochemistry of El Valle Volcano, Panama: Contributions to Mineralogy and Petrology, v. 106, p. 309–324, doi: 10.1007/BF00324560.

Defant, M.J., Richerson, P.M., de Boer, J.Z., Stewart, R.H., Maury, R.C., Bellon, H., Drummond, M.S., Feigenson, M.D., and Jackson, T.E., 1991b, Dacite genesis via both slab melting and differentiation: Petrogenesis of La Yeguada Volcanic Complex, Panama: Journal of Petrology, v. 32, p. 1101–1142.

Defant, M.J., Jackson, T.E., Drummond, M.S., de Boer, J.Z., Bellon, H., Feigenson, M.D., Maury, R.C., and Stewart, R.H., 1992, The geochemistry of young volcanism throughout western Panama and southeastern Costa Rica: An overview: Journal of the Geological Society of London, v. 149, no. 4, p. 569–579, doi: 10.1144/gsjgs.149.4.0569.

Dorendorf, F., Wiechert, U., and Worner, G., 2000, Hydrated sub-arc mantle: A source for the Kluchevskoy volcano, Kamchatka/Russia: Earth and Planetary Science Letters, v. 175, p. 69–86, doi: 10.1016/S0012-821X(99)00288-5.

Drummond, M.S., Bordelon, M., de Boer, J.Z., Defant, M.J., Bellon, H., and Feigenson, M.D., 1995, Igneous petrogenesis and tectonic setting of plutonic and volcanic rocks of the Cordillera de Talamanca, Costa Rica-Panama, Central American arc: American Journal of Science, v. 295, p. 875–919.

Duncan, R.A., and Hargraves, R.B., 1984, Plate tectonic evolution of the Caribbean region in the mantle reference frame, *in* Bobini, W.E., Hargraves, R.B., and Shagam, R., eds., The Caribbean Plate Boundary and Regional Tectonics: Geological Society of America Memoir 162, p. 81–93.

Duque-Caro, H., 1990, The choco block in the northwestern corner of South America: Structural, tectonostratigraphic, and paleogeographic implications: Journal of South American Earth Sciences, v. 3, p. 71–84, doi: 10.1016/0895-9811(90)90019-W.

Eiler, J.M., Farley, K.A., Valley, J.W., Hofmann, A.W., and Stolper, E.M., 1996, Oxygen isotope constraints on the sources of Hawaiian volcanism: Earth and Planetary Science Letters, v. 144, no. 3–4, p. 453–467, doi: 10.1016/S0012-821X(96)00170-7.

Eiler, J.M., Farley, K.A., Valley, J.W., Hauri, E., Craig, H., Hart, S.R., and Stolper, E.M., 1997, Oxygen isotope variations in ocean island basalt phenocrysts: Geochimica et Cosmochimica Acta, v. 61, p. 2281–2293, doi: 10.1016/S0016-7037(97)00075-6.

Eiler, J.M., Grönvold, K., and Kitchen, N., 2000, Oxygen isotope evidence for the origin of chemical variations in lavas from Theistareykir volcano in Iceland's northern volcanic zone: Earth and Planetary Science Letters, v. 184, p. 269–286, doi: 10.1016/S0012-821X(00)00318-6.

Feigenson, M.D., Carr, M.J., Maharaj, S.V., Juliano, S., and Bolge, L.L., 2004, Lead isotope composition of Central American volcanoes: Influence of the Galápagos plume: Geochemistry Geophysics Geosystems, v. 5, p. Q06001, doi: 10.1029/2003GC000621.

Fisher, S.P., and Pessagno, E.A., 1965, Upper Cretaceous strata of northwestern Panama: American Association of Petroleum Geologists Bulletin, v. 49, p. 433–444.

Gazel, E., Carr, M. J., Hoernle, K., Feigenson, M. D., Szymanski, D., Hauff, F., and van den Bogaard, P., 2009, Galápagos-OIB signature in southern Central America: Mantle refertilization by arc-hotspot interaction: Geochemistry Geophysics Geosystems, v. 10, p. Q02S11.

Goossens, P.J., Rose, W.I.J., and Flores, D., 1977, Geochemistry of tholeiites of the Basic Igneous Complex of northwestern South America: Geological Society of America Bulletin, v. 88, p. 1711–1720, doi: 10.1130/0016-7606(1977)88<1711:GOTOTB>2.0.CO;2.

Gregory, R.T., Criss, R.E., and Taylor, H.P., 1989, Oxygen isotope exchange kinetics in mineral pairs in closed and open systems: Application to problems of hydrothermal alteration and Precambrian Iron Formations: Chemical Geology, v. 75, p. 1–42, doi: 10.1016/0009-2541(89)90019-3.

Harmon, R.S., and Gerbe, M.-C., 1992, The 1982–83 eruption at Galunggung Volcano, Java (Indonesia): Oxygen isotope geochemistry of a chemically zoned magma chamber: Journal of Petrology, v. 33, p. 585–609.

Harmon, R.S., Hoefs, J., and Wedepohl, K.-H., 1987, Stable isotope (O, H, S) relationships in Tertiary basalts and their mantle xenoliths from the Northern Hessian Depression, W. Germany: Contributions to Mineralogy and Petrology, v. 95, p. 350–369, doi: 10.1007/BF00371849.

Hauff, F., Hoernle, K., Schmincke, H.U., and Werner, R., 1997, A mid Cretaceous origin for the Galápagos hotspot: volcanological, petrological and geochemical evidence from Costa Rican oceanic crustal segments: Geologische Rundschau, v. 86, p. 141–155, doi: 10.1007/PL00009938.

Hauff, F., Hoernle, K., van den Bogaard, P., Alvarado, G., and Garbe-Schönberg, D., 2000a, Age and geochemistry of basaltic complexes in western Costa Rica: Contributions to the geotectonic evolution of Central America: Geochemistry Geophysics Geosystems, v. 1, p. 1009, doi: 10.1029/1999GC000020.

Hauff, F., Hoernle, K., Tilton, G., Graham, D., and Kerr, A.C., 2000b, Large volume recycling of oceanic lithosphere over short time scales: geochemical constraints from the Caribbean large igneous province: Earth and Planetary Science Letters, v. 174, p. 247–263, doi: 10.1016/S0012-821X(99)00272-1.

Haug, G.H., and Tiedemann, R., 1998, Effect of the formation of the Isthmus of Panama on Atlantic Ocean thermohaline circulation: Nature, v. 393, p. 673–676, doi: 10.1038/31447.

Haug, G.H., Tiedemann, R., Zahn, R., and Ravelo, A.C., 2001, Role of Panama uplift on oceanic freshwater balance: Geology, v. 29, no. 3, p. 207–210, doi: 10.1130/0091-7613(2001)029<0207:ROPUOO>2.0.CO;2.

Heinrichs, H., and Herrmann, A.G., 1990, Praktikum der analytischen Geochemie, Springer-Lehrbuch: Berlin, Springer-Verlag, 669 p.

Hoernle, K., and Hauff, F., 2007, Oceanic igneous complexes, *in* Bundschuh, J., and Avarado, G., eds., Central America: Geology, Resources and Hazards: Lisse, Swets and Zeitlinger, p. 523–547.

Hoernle, K., Werner, R., Morgen, J.P., Garbe-Schönberg, D., Bryce, J., and Mrazek, J., 2000, Existence of complex spatial zonation in the Galápagos plume: Geology, v. 28, p. 435–438, doi: 10.1130/0091-7613(2000)28<435:EOCSZI>2.0.CO;2.

Hoernle, K., van den Bogaard, P., Werner, R., Lissinna, B., Hauff, F., Alvarado, G., and Garbe-Schönberg, D., 2002, Missing history (16–71 Ma) of the Galápagos hotspot: Implications for the tectonic and biological evolution of the Americas: Geology, v. 30, p. 795–798, doi: 10.1130/0091-7613(2002)030<0795:MHMOTG>2.0.CO;2.

Hoernle, K., Hauff, F., and van den Bogaard, P., 2004, 70 m.y. history (139–69 Ma) for the Caribbean large igneous province: Geology, v. 32, p. 697–700, doi: 10.1130/G20574.1.

Hoernle, K., Abt, D.L., Fischer, K.M., Nichols, H., Hauff, F., Abers, G.A., van den Bogaard, P., Heydolph, K., Alvarado, G., Protti, M., and Strauch, W., 2008, Arc-parallel flow in the mantle wedge beneath Costa Rica and Nicaragua: Nature, v. 451, p. 1094–1097, doi: 10.1038/nature06550.

Ionov, D.A., Harmon, R.S., France-Lanord, C., Greenwood, P.B., and Ashchepkov, I.V., 1994, Oxygen isotope composition of garnet and spinel peridotites in the continental mantle: Evidence from the Vitim xenolith suite, southern Siberia: Geochimica et Cosmochimica Acta, v. 58, p. 1463–1470, doi: 10.1016/0016-7037(94)90549-5.

Johnston, S.T., and Thorkelson, D.J., 1997, Cocos-Nazca slab window beneath Central America: Earth and Planetary Science Letters, v. 146, p. 465–474, doi: 10.1016/S0012-821X(96)00242-7.

Kay, R.W., 1978, Aleutian magnesian andesites: Melts from subducted Pacific ocean crust: Journal of Volcanology and Geothermal Research, v. 4, p. 117–132, doi: 10.1016/0377-0273(78)90032-X.

Kerr, A.C., Marriner, G.F., Tarney, J., Nivia, A., Saunders, A.D., Thirlwall, M.F., and Sinton, C.W., 1997, Cretaceous basaltic terranes in western Colombia: Elemental, chronological and Sr-Nd isotopic constraints on petrogenesis: Journal of Petrology, v. 38, p. 677–702, doi: 10.1093/petrology/38.6.677.

Kerr, A.C., Tarney, J., Kempton, P.D., Spadea, P., Nivia, A., Marriner, G.F., and Duncan, R.A., 2002, Pervasive mantle plume head heterogeneity: Evidence from the late Cretaceous Caribbean-Colombian oceanic plateau: Journal of Geophysical Research, v. 107, doi: 10.1029/2001JB000790.

Kesler, S.E., Sutter, J.F., Issigonis, M.J., Jones, L.M., and Walker, R.L., 1977, Evolution of porphyry copper mineralization in an oceanic island arc; Panama: Economic Geology and the Bulletin of the Society of Economic Geologists, v. 72, p. 1142–1153.

Kieffer, S.W., 1982, Thermodynamics and lattice-vibrations of minerals: 5. Applications to phase equilibria, isotope fractionation and high-pressure thermodynamic properties: Reviews of Geophysics, v. 20, p. 827–849, doi: 10.1029/RG020i004p00827.

Lapierre, H., Dupuis, V., de Mercier, L.B., Bosch, D., Monie, P., Tardy, M., Maury, R.C., Hernandez, J., Polve, M., Yeghicheyan, D., and Cotten, J., 1999, Late Jurassic oceanic crust and Upper Cretaceous Caribbean Plateau picritic basalts exposed in the Duarte Igneous Complex, Hispaniola: A reply: The Journal of Geology, v. 107, p. 509–512, doi: 10.1086/314362.

Le Maitre, R.W., Bateman, P., Dudek, A., Keller, J., Lemeyre, J., Le Bas, M., Sabine, P., Schmid, R., Sorensen, H., Streckeisen, A., Wooley, A., and Zanettin, B., 1989, A classification of igneous rocks and glossary of terms: Oxford, Blackwell Publishing, 193 p.

Lissinna, B., Hoernle, K., Hauff, F., van den Bogaard, P., and Sadofsky, S., 2006, The Panamanian island arc and Galápagos hotspot: A case study for the long-term evolution of arc/hotspot interaction: Geophysical Research Abstracts, Copernicus Group.

Lonsdale, P., 2005, Creation of the Cocos and Nazca plates by fission of the Farallon plate: Tectonophysics, v. 404, p. 237–264, doi: 10.1016/j.tecto.2005.05.011.

Lonsdale, P., and Klitgord, K.D., 1978, Structure and tectonic history of the eastern Panama Basin: Geological Society of America Bulletin, v. 89, p. 981–999, doi: 10.1130/0016-7606(1978)89<981:SATHOT>2.0.CO;2.

MacMillan, I., Gans, P.B., and Alvarado-Induni, G.E., 2004, Middle Miocene to present plate tectonic history of the southern Central American Volcanic Arc: Tectonophysics, v. 392, p. 325–348, doi: 10.1016/j.tecto.2004.04.014.

Mann, P., and Kolarsky, R., 1995, East Panama deformed belt; structure, age, and neotectonic significance, *in* Mann, P., ed., Geologic and Tectonic Development of the Caribbean Plate Boundary in Southern Central America: Geological Society of America Special Paper 262, p. 111–130.

Matsuhisa, Y., 1979, Oxygen isotopic compositions of volcanic rocks from the east Japan island arcs and their bearing on petrogenesis: Journal of Volcanology and Geothermal Research, v. 5, p. 271–296, doi: 10.1016/0377-0273(79)90020-9.

Mattey, D., Lowry, D., and Macpherson, C., 1994, Oxygen isotope composition of mantle peridotite: Earth and Planetary Science Letters, v. 128, p. 231–241, doi: 10.1016/0012-821X(94)90147-3.

Matthews, A., Goldsmith, J.R., and Clayton, R.N., 1983, Oxygen isotope fractionations involving pyroxenes: The calibration of mineral-pair geothermometers: Geochimica et Cosmochimica Acta, v. 47, p. 631–644, doi: 10.1016/0016-7037(83)90284-3.

Maury, R.C., Defant, M.J., Bellon, H., de Boer, J.Z., Stewart, R.H., and Cotton, J., 1995, Early Tertiary arc volcanics from eastern Panama, *in* Mann, P., ed., Geologic and Tectonic Development of the Caribbean Plate Boundary in Southern Central America: Geological Society of America Special Paper 295, p. 29–34.

Meschede, M., and Frisch, W., 1998, A plate-tectonic model for the Mesozoic and Early Cenozoic history of the Caribbean plate: Tectonophysics, v. 296, no. 3–4, p. 269–291, doi: 10.1016/S0040-1951(98)00157-7.

Muehlenbachs, K., and Clayton, R.N., 1972, Oxygen isotope studies of fresh and weathered submarine basalts: Canadian Journal of Earth Sciences, v. 9, p. 471–479.

Pack, A., Toulouse, C., and Przybilla, R., 2007, Determination of oxygen triple isotope ratios of silicates without cryogenic separation of NF3-technique with application to analyzes of technical O_2 gas and meteorite classification: Rapid Communications in Mass Spectrometry, v. 21, p. 3721–3728, doi: 10.1002/rcm.3269.

PetDB (Petrological Database of the Ocean Floor), 2008, http://www.petdb.org/petdbWeb/search/download_pg.jsp, online source.

Pindell, J., Kennan, L., Maresch, M.W., Stanek, K.P., Draper, G., and Higgs, R., 2005, Plate-kinematics and crustal dynamics of circum-Caribbean arc-continent interactions: Tectonic controls an basin development in proto–Caribbean margins, *in* Lallemant, H.G.A., and

Sisson, V.B., eds., Caribbean–South American Plate Interactions, Venezuela: Geological Society of America Special Paper 394, p. 7–52.

Pindell, J., Kennan, L., Stanek, K.P., Maresch, M.W., and Draper, G., 2006, Foundations of Gulf of Mexico and Caribbean evolution: Eight controversies resolved: Geological Acta, v. 4, p. 303–341.

Plank, T., and Langmuir, C.H., 1998, The chemical composition of subducting sediment and its consequences for the crust and mantle: Chemical Geology, v. 145, p. 325–394, doi: 10.1016/S0009-2541(97)00150-2.

Recchi, J., 1975, Paleografia Atlas Nacional de Panamá: Instituto Geografico Nacional "Tommy Guardia," 128 p.

Renne, P.R., Swisher, C.C., Deino, A.L., Karner, D.B., Owens, T.L., and DePaolo, D.J., 1998, Intercalibration of standards, absolute ages and uncertainties in $^{40}Ar/^{39}Ar$ dating: Chemical Geology, v. 145, p. 117–152, doi: 10.1016/S0009-2541(97)00159-9.

Revillon, S., Arndt, N.T., Chauvel, C., and Hallot, E., 2000a, Geochemical study of ultramafic volcanic and plutonic rocks from Gorgona Island, Colombia: The plumbing system of an oceanic plateau: Journal of Petrology, v. 41, no. 7, p. 1127–1153, doi: 10.1093/petrology/41.7.1127.

Reynaud, C., Jaillard, É., Lapierre, H., Mamberti, M., and Mascle, G.H., 1999, Oceanic plateau and island arcs of southwestern Ecuador: Their place in the geodynamic evolution of northwestern South America: Tectonophysics, v. 307, p. 235–254, doi: 10.1016/S0040-1951(99)00099-2.

Rickwood, P.C., 1989, Boundary lines within petrologic diagrams which use oxides of major and minor elements: Lithos, v. 22, no. 4, p. 247–263, doi: 10.1016/0024-4937(89)90028-5.

Sadofsky, S., Hoernle, K., Duggen, S., Hauff, F., Werner, R., and Garbe-Schönberg, D., 2009, Geochemical variations in the Cocos plate subducting beneath Central America: Implications for the composition of arc volcanism and the extent of the Galápagos hotspot influence on the Cocos oceanic crust: International Journal of Earth Sciences, v. 98, p. 901–913, doi: 10.1007/s00531-007-0289-5.

Sharp, Z.D., 1990, A laser-based microanalytical method for the in situ determination of oxygen isotope ratios of silicates and oxides: Geochimica et Cosmochimica Acta, v. 54, p. 1353–1357, doi: 10.1016/0016-7037(90)90160-M.

Sinton, C.W., Christie, D.M., and Duncan, R.A., 1996, Geochronology of Galápagos seamounts: Journal of Geophysical Research, v. 101, p. 13,689–13,700, doi: 10.1029/96JB00642.

Sinton, C.W., Duncan, R.A., and Denyer, P., 1997, Nicoya Peninsula, Costa Rica: A single suite of Caribbean oceanic plateau magmas: Journal of Geophysical Research, v. 102, p. 15507–15520, doi: 10.1029/97JB00681.

Sinton, C.W., Duncan, R.A., Storey, M., Lewis, J., and Estrada, J.J., 1998, An oceanic flood basalt province within the Caribbean plate: Earth and Planetary Science Letters, v. 155, p. 221–235, doi: 10.1016/S0012-821X(97)00214-8.

Smith, M.E., Singer, B.S., Carroll, A.R., and Fournelle, J.H., 2006, High-resolution calibration of Eocene strata: $^{40}Ar/^{39}Ar$ geochronology of biotite in the Green River Formation: Geology, v. 34, p. 393–396, doi: 10.1130/G22265.1.

Steiger, R.H., and Jäger, E., 1977, Subcommission on geochronology: Convention on the use of decay constants in geo- and cosmochronology: Earth and Planetary Science Letters, v. 36, p. 359–362, doi: 10.1016/0012-821X(77)90060-7.

Stern, C.R., and Kilian, R., 1996, Role of the subducted slab, mantle wedge, and continental crust in the generation adakites from the Andean Austral volcanic zone: Contributions to Mineralogy and Petrology, v. 123, p. 263–281, doi: 10.1007/s004100050155.

Sun, S.S., and McDonough, W.F., 1989, Chemical and isotopic systematics of oceanic basalts: Implications for mantle composition and processes: The Geological Society of London, Special Publications, v. 42, p. 313–345.

Taylor, H.P., Turi, B., and Cundari, A., 1984, $^{18}O/^{16}O$ and chemical relationships in K-rich volcanic rocks from Australia, East Africa, Antarctica, and San Venanzo Cupaello, Italy: Earth and Planetary Science Letters, v. 69, p. 263–276, doi: 10.1016/0012-821X(84)90186-9.

Weyl, R., 1980, Geology of Central America (2nd edition): Berlin-Stuttgart, Gebrueder Borntraeger, 371 p.

White, W.M., McBirney, A.R., and Duncan, R.A., 1993, Petrology and geochemistry of the Galápagos Islands: Portrait of a pathological mantle plume: Journal of Geophysical Research, v. 98, p. 19,533–19,563, doi: 10.1029/93JB02018.

Wörner, G., Harmon, R., Hartmann, G., and Simon, K., 2005, Igneous geology and geochemistry of the Upper Río Chagres Basin, *in* Harmon, R.S., ed., The Río Chagres, Panama: A Multidisciplinary Profile of a Tropical Watershed: Amsterdam, Springer, p. 65–81.

Wörner, G., Harmon, R.S., and Wegner, W., 2009, Geochemical evolution of igneous rock and changing magma sources during the evolution and closure of the Central American Landbridge, *in* Kay, S.M., Ramos, V.A., and Dickinson, W.R., eds., Backbone of the Americas: Shallow Subduction, Plateau Uplift, and Ridge and Terrane Collision: Geological Society of America Memoir 204, p. 183–196.

Zhao, Z.-F., and Zheng, Y.-F., 2002, Calculation of O-isotope fractionation in magmatic rocks: Chemical Geology, v. 193, p. 59–80, doi: 10.1016/S0009-2541(02)00226-7.

Zheng, Y.-F., 1991, Calculation of oxygen isotope fractionation in metal oxides: Geochimica et Cosmochimica Acta, v. 55, p. 2299–2307, doi: 10.1016/0016-7037(91)90105-E.

Zheng, Y.-F., 1997, Prediction of high-temperature oxygen isotope fractionation factors between mantle minerals: Physics and Chemistry of Minerals, v. 24, p. 356–364, doi: 10.1007/s002690050049.

Zindler, A., and Hart, S., 1986, Chemical geodynamics: Annual Review of Earth and Planetary Sciences, v. 14, p. 493–571, doi: 10.1146/annurev.ea.14.050186.002425.

Manuscript Received 18 June 2009
Revised Manuscript Received 25 November 2009
Manuscript Accepted 6 December 2009

Printed in the USA